

Model Predictive Communication for Timely Status Updates in Low-Altitude Networks

Bowen Li, Jiping Luo, Themistoklis Charalambous, Nikolaos Pappas

Abstract—Timely information delivery in low-altitude networks is critical for many time-sensitive applications, such as unmanned aerial vehicle (UAV) navigation, inspection, and surveillance. The key challenge lies in balancing three competing factors: stringent data freshness requirements, UAV onboard energy consumption, and interference with terrestrial services. Addressing this challenge requires not only efficient power and channel allocation strategies but also effective communication timing over the entire operation horizon. In this work, we propose a model predictive communication (MPComm) framework, enabled by advanced channel sensing techniques, in which the channel conditions that the UAV will experience are largely predictable. Within this framework, we formulate a constrained bi-objective optimization problem to achieve a desired trade-off between energy consumption and terrestrial channel occupation, subject to a strict timeliness constraint. We solve this problem using Pareto analysis and show that the original non-convex, mixed-integer problem can be decomposed into a two-layer structure: the outer layer determines the optimal communication timing, while the inner layer determines the optimal power and channel allocation for each communication interval. An efficient algorithm for the inner problem is developed using non-convex analysis, with asymptotic optimality guarantees, while the outer problem is solved optimally via a simple graph search, with edges characterized by inner solutions. The proposed approach applies to a broad class of problem variants, including objective transformations and single-objective specializations. Numerical results demonstrate the efficiency of the proposed solution, achieving up to a six-fold reduction in terrestrial channel occupation and a 6dB energy saving compared to benchmark schemes.

Index Terms—Low-altitude networks, UAV communications, Model predictive communication, and timely status updates.

I. Introduction

Low-altitude activities have grown significantly over the past decade, leading to a surge in demand for timely communications that support time-critical applications such as real-time navigation, inspection, and surveillance [1]. In such applications, stringent data freshness requirements are typically imposed [2], [3]. For instance, timely access to unmanned aerial vehicle (UAV) sensory data is essential for aerial traffic coordination, mission

monitoring, and decision-making at the control center; obsolete information can degrade operational safety and even lead to crashes.

Most existing works on aerial communications focus on the throughput-reliability-delay trade-off [4], [5]. However, such approaches may not suffice for many safety-critical applications. UAVs typically face strict energy constraints and limited communication budgets. It is inefficient, if not impossible, to communicate every piece of sensory data to the control center. Instead, the most recent and relevant data should be generated and delivered promptly [6]. A natural question then arises: What is the optimal timing of communication? The answer is not obvious, especially in low-altitude networks where channel conditions and network topology can change rapidly. Recent studies [7]–[9] have investigated this problem from information-theoretic and control-theoretic perspectives. Intuitively, transmitting immediately, given abundant communication resources, may be a bad timing if better channel conditions are expected in the near future. In this article, we employ the age of information (AoI) metric [6] as an indicator of data freshness and address this question by proposing a predictive communication strategy.

Low-altitude networks, while dynamic, are often predictable [10]. First, in many applications such as inspection and cargo delivery, UAVs follow predetermined trajectories and their future movements are largely predictable [11]. Second, advanced channel sensing techniques, such as radio maps and digital twins [12]–[14], provide predictable and high-precision 3D representations of the wireless propagation environment. In such applications, the communication model can be predicted with reasonable accuracy. This enables model predictive communication (MPComm), where resource management, data acquisition, and access control are optimized over a longer planning horizon. Recently, some preliminary results have demonstrated the effectiveness of MPComm on routing, resource allocation, beamforming, and local negotiation in low-altitude UAV networks [15]–[20].

There are several key trade-offs in the design of low-altitude, timely communication networks. The first trade-off is between UAV energy consumption and the quality of service (QoS) of terrestrial services. The coexistence of aerial and terrestrial traffic is complicated by dominant line-of-sight (LOS) channels, which induce severe cross-network interference [21], [22]. Consequently, improving aerial communication throughput generally requires either more onboard energy or more terrestrial spectrum

Part of this work will be presented at the IEEE ICC 2026.

This work has been supported by ELLIIT and 6G-LEADER, 101192080.

B. Li, J. Luo, and N. Pappas are with the Department of Computer and Information Science, Linköping University, 58183 Linköping, Sweden. Emails: {bowen.li, jiping.luo, nikolaos.pappas}@liu.se

T. Charalambous is with the Department of Electrical and Computer Engineering, University of Cyprus, 1678 Nicosia, Cyprus. Email: charalambous.themistoklis@ucy.ac.cy

resources. The system therefore trades UAV energy consumption against the QoS of terrestrial services. The second trade-off is between resource utilization cost and data freshness. To meet stringent timeliness constraints, appropriate sample/communication timing and resource allocation decisions must be made.

Many existing works focus on UAV trajectory optimization and resource allocation to minimize AoI in data collection tasks [23]–[28]. However, most of them adopt packet-level metrics that measure the lifetime of each update, which is insufficient for time-critical tasks such as UAV status monitoring. Another line of research adopts source-level metrics to characterize the freshness of the information at the remote center [29]–[32]. Nevertheless, these works do not exploit the predictability of low-altitude networks and therefore remain essentially reactive rather than proactive.

In this work, we formulate a bi-objective optimization problem within the MPCComm framework to achieve a desired trade-off between aerial energy consumption and terrestrial spectrum usage, subject to a hard timeliness constraint on aerial traffic. The decision variables include the timing of status updates, the UAV’s power allocation, and the occupation of terrestrial spectrum. These decisions are optimized over a long planning horizon to adapt to predicted channel conditions. This constrained bi-objective problem poses two main challenges: (i) it is a non-convex, mixed-integer program, and (ii) its complete solution constitutes a Pareto frontier, which is computationally challenging to obtain. We propose a low-complexity method to address these challenges.

Our main contributions are summarized below.

(1) We propose an MPCComm framework for timely status updates in low-altitude networks. Within this framework, we formulate a constrained bi-objective optimization problem to satisfy data freshness requirements while balancing energy consumption and terrestrial channel usage. Unlike conventional designs that focus solely on data transmission, the proposed framework directly controls information generation and transmission through an age-aware sampling controller.

(2) We exploit the problem structure to characterize the Pareto frontier and derive tight upper and lower bounds for its region. These results significantly reduce computation overhead. We further show that, for general formulations with objective transformations, the frontier in the transformed objective space can be obtained directly as a simple transformation of the original frontier. In addition, solutions for weighted-sum and constrained formulations lie on the frontier, enabling efficient solution retrieval.

(3) We develop an efficient algorithm to solve the bi-objective problem. The problem is first decomposed into a two-layer structure, where the outer layer determines the optimal communication timing, while the inner layer determines the optimal power and channel allocation for each communication interval. Leveraging this decomposition and non-convex analysis, we propose

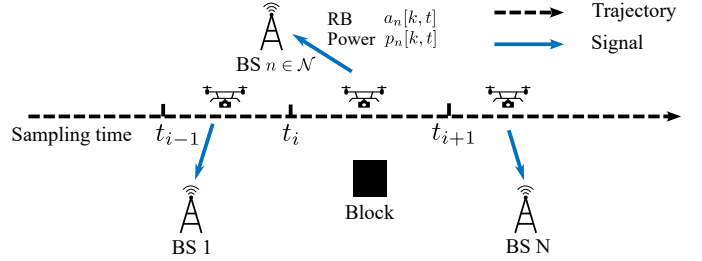


Fig. 1. Illustration of the UAV telemetry system. The UAV symbols along the trajectory illustrate the UAV’s positions at different time instants. The UAV reports on-board data to a control center through BSs.

a graph-based algorithm with complexity linear in the number of base stations (BSs) and planning horizon, and quadratic in the number of channel resource blocks (RBs). Numerical results demonstrate that the proposed solution achieves up to a six-fold reduction in terrestrial channel occupation and a 6 dB energy saving compared to benchmark solutions.

The rest of the paper is organized as follows. Section II introduces the MPCComm framework. Section III characterizes the Pareto frontier and decomposes the optimization problem. Section IV develops a graph-based algorithm. Section V introduces the variant problems and discusses their connections to the original problem. Numerical results are provided in Section VI, and we conclude this paper in Section VII.

Notation: Let \mathbb{R} , \mathbb{R}_+ , \mathbb{Z} , and \mathbb{Z}_+ denote the sets of real numbers, nonnegative real numbers, integers, and nonnegative integers, respectively. Calligraphic letters denote sets or index sets, e.g., $\mathcal{N} \triangleq \{1, \dots, N\}$, $\mathcal{K} \triangleq \{1, \dots, K\}$, and $\mathcal{T} \triangleq \{1, \dots, T\}$, with $|\mathcal{N}|$ denoting the cardinality of \mathcal{N} and \mathcal{N}^K denoting the K -fold Cartesian product of \mathcal{N} . Bold lowercase letters, bold uppercase letters, and bold calligraphic letters denote vectors, matrices, and tensors, respectively. For example, for a third-order tensor $\mathcal{X} \in \mathbb{R}^{N \times K \times T}$ with entries $x_n[k, t]$, we write $\mathcal{X} = \{x_n[k, t]\}_{n \in \mathcal{N}, k \in \mathcal{K}, t \in \mathcal{T}}$, $\mathbf{X}_n = \{x_n[k, t]\}_{k \in \mathcal{K}, t \in \mathcal{T}} \in \mathbb{R}^{K \times T}$, $\mathbf{X}[t] = \{x_n[k, t]\}_{n \in \mathcal{N}, k \in \mathcal{K}} \in \mathbb{R}^{N \times K}$, $\mathbf{X}[k] = \{x_n[k, t]\}_{n \in \mathcal{N}, t \in \mathcal{T}} \in \mathbb{R}^{N \times T}$, and $\mathbf{x}_{n,k} = \{x_n[k, t]\}_{t \in \mathcal{T}} \in \mathbb{R}^T$. For $x, a \in \mathbb{R}$, $x \rightarrow a^-$ and $x \rightarrow a^+$ denote that x approaches a from the left and from the right, respectively.

II. System Model

Consider a UAV telemetry system, as depicted in Fig. 1. The system consists of one UAV indexed by 0, and N BSs indexed by $n \in \mathcal{N} = \{1, \dots, N\}$. The UAV updates its on-board sensory data to a control center via the terrestrial network (i.e., the BSs). Timely delivery of this information is crucial, as the control center relies on the most recent and relevant data for reliable analysis and informed decision-making. Meanwhile, the terrestrial network shall also maintain stable service for the ground users. The MPCComm framework is detailed below.

A. Predictive Channel Model

We consider a slotted orthogonal frequency division multiplexing (OFDM) system, where time is divided into slots indexed by $t \in \mathcal{T} = \{1, \dots, T\}$, and the available spectrum is partitioned into K orthogonal RBs, indexed by $k \in \mathcal{K} = \{1, \dots, K\}$. The wireless channel from the UAV to BS n on RB k at time t can be modeled as

$$h_n[k, t] = g_n[k, t] \xi_n[k, t], \quad (1)$$

where $g_n[k, t]$ is the large-scale channel gain (e.g., path loss and shadowing), and $\xi_n[k, t]$ is the small-scale fading following the Gamma distribution with unit mean [16], [33], i.e., $\xi_n[k, t] \sim \text{Gamma}(\kappa_n[k, t], 1/\kappa_n[k, t])$, where $\kappa_n[k, t]$ denotes the shape parameter and $1/\kappa_n[k, t]$ denotes scale parameter. The resulting channel model is obtained as

$$h_n[k, t] \sim \text{Gamma}(\kappa_n[k, t], g_n[k, t]/\kappa_n[k, t]). \quad (2)$$

The predictive channel model is built on two key enablers.

- advanced channel sensing techniques, such as radio maps and digital twins [12]–[14], which provide a 3D representation of the wireless propagation environment and offer spatially resolved channel statistics between the UAV and ground BSs; and
- high-precision UAV control, which allows the UAV to follow pre-determined trajectories $\{(t, \mathbf{p}_0[t])\}_{t \in \mathcal{T}}$ with minimal deviation [10], [11].

Consequently, the UAV's motion traces a one-dimensional slice through the 3D channel field, yielding a time-indexed channel profile that can be predicted in advance. Let

$$\{g_n[k, t], \kappa_n[k, t]\}_{k \in \mathcal{K}} \triangleq \Xi(\mathbf{p}_0[t], \mathbf{p}_n), \quad \forall t \in \mathcal{T}, \quad (3)$$

denote the radio map between the UAV and BS n with position \mathbf{p}_n along the trajectory. The predictive channel information is available to the control center prior to deployment.

B. Communication Model

Denote by $a_n[k, t] \in \{0, 1\}$ the indicator of allocating RB k at slot t for the transmission from the UAV to BS n . For each RB (k, t) , the transmitting UAV can be scheduled to at most one BS, i.e., $\sum_{n \in \mathcal{N}} a_n[k, t] \leq 1$. Accordingly, the RB scheduling policy $\mathbf{A}[t]$ for any time $t \in \mathcal{T}$ is restricted to the feasible set

$$\mathcal{S}_{\mathbf{A}} \triangleq \left\{ \mathbf{A} \in \{0, 1\}^{|\mathcal{N}| \times |\mathcal{K}|} : \sum_{n \in \mathcal{N}} a_n[k, t] \leq 1, \forall k \in \mathcal{K} \right\}. \quad (4)$$

Let $p_n[k, t] \geq 0$ denote the transmit power of the UAV associated with (n, k, t) . The total transmission power is limited to the threshold \bar{p} , leading to the sum-power constraint $\mathbf{P}[t] \in \mathcal{S}_{\mathbf{P}}$, where $\mathcal{S}_{\mathbf{P}}$ denotes the feasible power set

$$\mathcal{S}_{\mathbf{P}} \triangleq \left\{ \mathbf{P} \in \mathbb{R}_+^{|\mathcal{N}| \times |\mathcal{K}|} : \sum_{n \in \mathcal{N}} \sum_{k \in \mathcal{K}} p_n[k, t] \leq \bar{p} \right\}. \quad (5)$$

We now derive the sum data rate. The signal-to-noise ratio (SNR) for the link from the UAV to BS n on RB k at time t is given by

$$\gamma_n[k, t] = \frac{p_n[k, t] h_n[k, t]}{\delta^2}, \quad (6)$$

where δ^2 is the noise power. We assume perfect Doppler compensation [34]. Then, the instantaneous channel capacity from the UAV to BS n at time t for RBs k is modeled as

$$c_n[k, t] = \log_2(1 + \gamma_n[k, t]). \quad (7)$$

Finally, the sum data rate over a time interval (t', t'') aggregated across all BSs and RBs is given by¹

$$v(t', t'') = \sum_{n \in \mathcal{N}} \sum_{k \in \mathcal{K}} \sum_{t=t'}^{t''-1} c_n[k, t] a_n[k, t]. \quad (8)$$

We note that $h_n[k, t]$, and hence $c_n[k, t]$ and $v(t', t'')$, are random variables. In the sequel, their expectations will be used in the performance evaluation.

C. Performance Metrics

1) Timeliness requirement for aerial traffic: In this work, we use the AoI metric to quantify the freshness of information received from the UAV [35]. Let $s[t] \in \{0, 1\}$ denote the update-success indicator for the UAV at the end of the slot t , and let G_t denote the generation time of the latest sample received at the receiver by time t . The AoI at the control center is recursively defined as

$$\tau[t+1] \triangleq \begin{cases} t - G_t, & s[t] = 1, \\ \tau[t] + 1, & s[t] = 0. \end{cases} \quad (9)$$

A transmission attempt is successful if the expected delivered payload accumulated since the previous success meets a quality threshold \bar{v} , i.e.,

$$s[t] = \mathbb{I}\{\mathbb{E}\{v(t_0, t)\} \geq \bar{v}\}. \quad (10)$$

Here, the expectation is with respect to the channel $h_n[k, t']$ for all $n \in \mathcal{N}$, $k \in \mathcal{K}$ and $t' \in [t_0, \dots, t-1]$.

For timeliness, we impose a hard constraint on the peak information age, i.e.,

$$\tau[t] \leq \bar{\tau}, \forall t \in \mathcal{T}, \quad (11)$$

where $\bar{\tau} \in \mathbb{Z}_+$. If the AoI exceeds the threshold, any ongoing incomplete transmission shall be aborted.

¹We assume reliable wired connectivity among the BSs/control center, so that the data received by different BSs can be aggregated cooperatively. A non-cooperative variant can be modeled by requiring that each update interval be delivered through only one BS. This variant preserves the problem structure and can be handled by the proposed algorithmic framework.

2) Fairness requirement for coexistence: We regulate the aerial load to ensure that each BS has sufficient spectrum resources for terrestrial services. The temporal load level at BS n is defined as the worst-case load occupied by aerial traffic,

$$l_n \triangleq \max_{t \in \mathcal{T}} \sum_{k \in \mathcal{K}} a_n[k, t].$$

We define the spatiotemporal load cap $\theta \in \mathbb{Z}_+$ as

$$\theta \triangleq \max_{n \in \mathcal{N}} l_n = \max_{n \in \mathcal{N}, t \in \mathcal{T}} \sum_{k \in \mathcal{K}} a_n[k, t]. \quad (12)$$

Equivalently, $K - \theta$ quantifies the worst-case residual spectrum available to terrestrial services.

3) Energy efficiency for aerial traffic: In contrast to ground BSs, which have a stable and sufficient energy supply, the energy consumption at the UAV is tightly constrained by its limited onboard battery capacity, making energy efficiency a critical design consideration. The energy consumption $E \in \mathbb{R}_+$ is defined as

$$E \triangleq \sum_{n \in \mathcal{N}, k \in \mathcal{K}, t \in \mathcal{T}} a_n[k, t] p_n[k, t]. \quad (13)$$

D. Problem Formulation

The goal is to maintain the timeliness of aerial traffic while balancing on-board energy consumption and spectrum usage. Let $\mathcal{P} = \{p_n[k, t]\}_{n \in \mathcal{N}, k \in \mathcal{K}, t \in \mathcal{T}}$ and $\mathcal{A} = \{a_n[k, t]\}_{n \in \mathcal{N}, k \in \mathcal{K}, t \in \mathcal{T}}$ denote the power allocation decisions and the RB allocation decisions over the entire planning horizon, respectively. We aim to solve the following constrained bi-objective problem²

$$\mathcal{P}1 : \underset{\pi \in [\mathcal{A}, \mathcal{P}]}{\text{minimize}} \quad \{\theta(\pi), E(\pi)\}, \quad (14)$$

$$\text{subject to } \tau[t] \leq \bar{\tau}, \forall t \in \mathcal{T}, \quad (15)$$

$$\pi \in \Pi \triangleq (\mathcal{S}_A \times \mathcal{S}_P)^{|\mathcal{T}|}, \quad (16)$$

where (14) includes the spectrum usage and on-board energy consumption objectives as defined in (12) and (13), (15) is the peak AoI constraint as defined in (9)–(11), and (16) is the feasible policy constraint specifying all admissible policies defined in (4)–(5).

A policy is feasible if it satisfies the peak AoI constraint. The challenge lies in finding the most effective policy that meets this constraint with minimal expenditure, thus preserving resources to optimize the objectives. This is referred to as the optimal communication timing problem, which will be made explicit in the next section.

The solution to $\mathcal{P}1$ is the complete Pareto frontier that consists of all Pareto-optimal strategies (see Definition 1). Each point on the frontier achieves a trade-off between the two competing objectives.

Definition 1: (Pareto optimality). A feasible strategy π^* is Pareto-optimal if there is no other feasible strategy $\pi \neq \pi^* \in \Pi$ such that $\theta(\pi') \leq \theta(\pi)$ and $E(\pi') \leq E(\pi)$ with

²Problem $\mathcal{P}1$ serves as a canonical formulation. We note that our analysis is applicable to a broad class of variants, as detailed in Section V.

at least one strict inequality. We refer to π^* as a Pareto-optimal policy in the decision space, and its objective image $\{\theta(\pi^*), E(\pi^*)\}$ as a Pareto-optimal point. The collections of all such policies and points constitute the Pareto-optimal set and the Pareto frontier, respectively.

Computing the exact Pareto frontier is a non-trivial task. First, the problem is a mixed-integer program, involving binary decision variables $a_n[k, t]$ and continuous decision variables $p_n[k, t]$. Second, the objectives and constraints are non-convex, which renders most existing algorithms ineffective or inapplicable. We will address this challenge in Section III and Section IV.

III. Pareto Analysis and Problem Decomposition

This section presents our main theoretical results on the Pareto frontier. We use the ϵ -constraint method ($\mathcal{P}2$) to characterize the frontier [36] and derive tight upper and lower bounds for its region. The peak AoI constraint in $\mathcal{P}2$ is then converted into a sum rate constraint that links age and communication timing ($\mathcal{P}3$). An important result, Proposition 1, shows that $\mathcal{P}3$ can be decomposed into a two-layer structure: the outer layer determines the optimal communication timing, while the inner layer finds the optimal resource allocation decisions for each given communication interval.

A. Characterization of the Pareto Frontier

We adopt the ϵ -constraint method to characterize the Pareto frontier. This choice is motivated by its theoretical completeness and practical implementability, particularly given the discrete nature of the system variables. In contrast, other common approaches, such as the weighted-sum method and the weighted L_p -norm method, may fail to capture non-convex regions of the frontier and can introduce additional complexity [36].

For a given $\varepsilon_\theta \in \mathcal{K}$, the ϵ -constraint method converts the bi-objective $\mathcal{P}1$ into a single-objective problem with multiple constraints. Formally, it is defined as

$$\mathcal{P}2 : \underset{\pi \in \Pi}{\text{min}} E(\pi), \text{ s.t. } \tau[t] \leq \bar{\tau}, \forall t \text{ and } \theta(\pi) \leq \varepsilon_\theta.$$

We next show that, for any given ε_θ within a certain range, the solution to $\mathcal{P}2$ is Pareto-optimal. Hence, by varying ε_θ over its feasible range, one can characterize the Pareto frontier of $\mathcal{P}1$. Since the load variable θ is integer-valued and finite, its feasible range is finite, making the sweep implementable. Furthermore, we derive tight bounds on θ to reduce computational overhead. These results are summarized in the following proposition.

Proposition 1 (Pareto frontier): The set

$$\mathcal{C} \triangleq \{(\varepsilon_\theta, E^*(\varepsilon_\theta)) : \varepsilon_\theta \in [\underline{\theta}, \bar{\theta}] \cap \mathbb{Z}_+\},$$

is the Pareto frontier of $\mathcal{P}1$, where $\underline{\theta} \triangleq \theta^*$,

$$\bar{\theta} \triangleq \min \{\varepsilon_\theta \in \mathbb{Z}_+ : E^*(\varepsilon_\theta) = E^*\}, \quad (17)$$

$E^*(\varepsilon_\theta)$ is the optimal value to $\mathcal{P}2$, and (θ^*, E^*) is the ideal point of $\mathcal{P}1$, i.e., the vector consisting of the separately attained optima of the two objectives.

Proof: See Appendix C. ■

B. Age-Aware Sampling Control

In this section, we convert the peak AoI constraint into a sum rate constraint that explicitly links age and sampling timing. Let t_i denote the sampling instant (i.e., data generation time) of the i th status packet of the UAV. The UAV starts the delivery process upon generation of a new status packet; any ongoing incomplete transmission shall be aborted. Let

$$\mathbf{t} = \{t_1, t_2, \dots, t_I\}$$

denote a sampling sequence over the entire horizon T , where

$$t_0 = 1, \quad 1 \leq t_1 < t_2, \dots < t_I \leq T, \quad (18)$$

and I is the total number of sampling events.

The peak AoI constraint in (11) implies that the sampling interval cannot exceed $\bar{\tau}$, that is,

$$1 \leq t_{i+1} - t_i \leq \bar{\tau}, \quad \forall i \in \mathcal{I}. \quad (19)$$

We set $t_{I+1} = T + 1$ to represent the end time of transmission for the I th status update. Therefore, the feasible sampling sequence is restricted by

$$\Upsilon = \left\{ \mathbf{t} \in \mathcal{T}^{|\mathcal{I}|} : 1 \leq t_{i+1} - t_i \leq \bar{\tau}, \forall i \in \mathcal{I} \right\}. \quad (20)$$

Recall that the transmission is successful if the sum rate satisfies (10). Accordingly, we impose the following expected sum rate constraint between any two consecutive sampling instances

$$\mathbb{E} \{v(t_i, t_{i+1})\} \geq \bar{v}, \quad \forall i \in \mathcal{I}. \quad (21)$$

As a result, the peak AoI constraint $\tau[t] \leq \bar{\tau}$ is converted into the sum rate constraint in (21) with $\mathbf{t} \in \Upsilon$. Then, $\mathcal{P}2$ is equivalent to the following problem

$$\mathcal{P}3 : \underset{\mathbf{A}, \mathcal{P}, \mathbf{t}}{\text{minimize}} \quad E(\boldsymbol{\pi}), \quad (22)$$

$$\text{s.t.} \quad \mathbb{E} \{v(t_i, t_{i+1})\} \geq \bar{v}, \forall i \in \mathcal{I}, \quad (23)$$

$$\theta(\boldsymbol{\pi}) \leq \varepsilon_\theta, \quad (24)$$

$$\mathbf{A} \in \mathcal{S}_A^{|\mathcal{T}|}, \mathcal{P} \in \mathcal{S}_P^{|\mathcal{T}|}, \mathbf{t} \in \Upsilon. \quad (25)$$

Fig. 2 illustrates that the age-aware sampling can reduce both RBs usage and energy consumption while maintaining the peak AoI constraint. An important implication is that age-aware sampling may involve more transmissions while using fewer resources by exploiting predictive channel information. More comparisons are presented in Section VI.

C. Problem Decomposition

Observe from problem $\mathcal{P}3$ that the variables are coupled over sampling instant \mathbf{t} by the objective function and constraint (23). Intuitively, given any feasible sampling variable sequence \mathbf{t} , $\mathcal{P}3$ can be decomposed into I parallel resource allocation subproblems. This result is formalized in the next theorem.

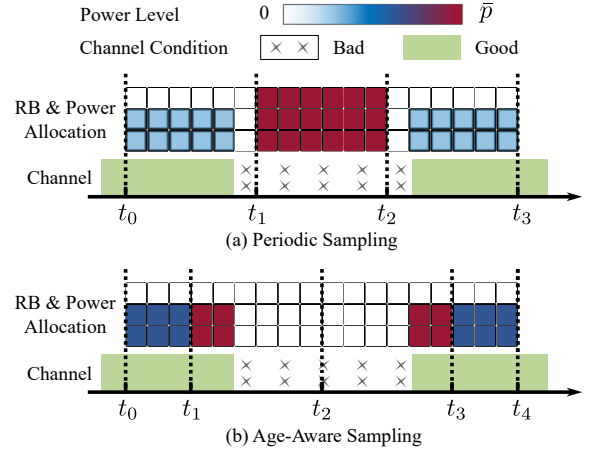


Fig. 2. Comparison of periodic and age-aware sampling policies. (a) The periodic policy communicates at a fixed rate and may violate the AoI constraint under poor channel conditions. (b) The age-aware policy adjusts its sampling time and resource allocation based on predictive channel information.

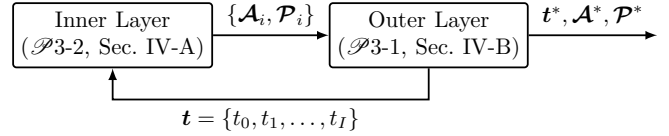


Fig. 3. Schematic representation of the two-layer structure.

Theorem 1 (Decomposition of $\mathcal{P}3$): Problem $\mathcal{P}3$ is equivalently transformed into the following outer subproblem

$$\mathcal{P}3-1 : \underset{\mathbf{t} \in \Upsilon}{\text{minimize}} \quad \sum_{i \in \mathcal{I}} E^*(t_i, t_{i+1}),$$

where $E^*(t_i, t_{i+1})$ is the solution to the inner subproblem

$$\begin{aligned} \mathcal{P}3-2 : \underset{\mathbf{A}_i, \mathcal{P}_i}{\text{minimize}} \quad & \sum_{n \in \mathcal{N}, k \in \mathcal{K}, t \in \mathcal{T}_i} a_n[k, t] p_n[k, t] \\ \text{subject to} \quad & \mathbb{E} \{v(t_i, t_{i+1})\} \geq \bar{v}, \\ & \sum_{k \in \mathcal{K}} a_n[k, t] \leq \varepsilon_\theta, \forall n \in \mathcal{N}, t \in \mathcal{T}_i, \\ & \mathbf{A}_i \in \mathcal{S}_A^{|\mathcal{T}_i|}, \mathcal{P}_i \in \mathcal{S}_P^{|\mathcal{T}_i|}, \end{aligned}$$

where $\mathcal{T}_i = [t_i, t_{i+1}) \cap \mathbb{Z}_+$ denotes the i th communication interval, and $\mathbf{A}_i = \{a_n[k, t]\}_{n \in \mathcal{N}, k \in \mathcal{K}, t \in \mathcal{T}_i}$ and $\mathcal{P}_i = \{p_n[k, t]\}_{n \in \mathcal{N}, k \in \mathcal{K}, t \in \mathcal{T}_i}$ are the RB and power allocation policy restricted to the time interval \mathcal{T}_i , respectively.

Proof: See Appendix A. \blacksquare

As depicted in Fig. 3, instead of directly solving the high-dimensional Problem $\mathcal{P}3$, we propose a two-layer structure that isolates the resource allocation problem ($\mathcal{P}3-2$) from the sampling control problem ($\mathcal{P}3-1$). Note that a sampling sequence \mathbf{t} is feasible if and only if all of its inner problems are feasible. The next section develops efficient algorithms to solve these sub-problems.

IV. Graph-Based Low-Complexity Algorithm

This section develops efficient algorithms to solve the decomposed subproblems $\mathcal{P}3-1$ and $\mathcal{P}3-2$. We first give

a brief overview of the proposed approach.

Section IV-A focuses on the inner problem of power and access control for a given communication interval. The main difficulty lies in the fact that $\mathcal{P}3$ -2 is a non-convex, mixed-integer program. To address this issue, we first relax the problem into a continuous-variable convex formulation $\mathcal{P}4$, which exhibits several convenient properties that can be leveraged to construct an optimal policy for $\mathcal{P}3$ -2 with reduced complexity. Based on these results, we develop an efficient algorithm, Algorithm 1, which is proven to achieve the global optimum in the high-SNR or strong-LOS regimes.

Section IV-B addresses the outer problem of sampling timing control. We show that $\mathcal{P}3$ -1 is equivalent to a shortest-path problem on a finite graph, where the weight of each edge corresponds to the solution of the inner problem for a given communication interval. A graph-based algorithm, Algorithm 2, is proposed to find an optimal sampling sequence.

A complexity analysis of the proposed algorithms is provided in Section IV-C. In particular, the overall complexity for computing the Pareto frontier is upper bounded by $\mathcal{O}(\bar{\tau}^2 N K^3 T \log(\epsilon^{-1}))$, which is linear in the number of BSs N , and the horizon length T , quadratic in the maximum AoI threshold $\bar{\tau}$, cubically with the number of RBs K , and logarithmically with the tolerable error tolerance ϵ .

A. Inner Solution: Power and Access Control

To resolve the inner problem $\mathcal{P}3$ -2, we first address the intractability of the stochastic sum rate constraint caused by channel randomness.

1) A Tractable Lower Bound of the Expected Sum Rate: The evaluation of the expectation $\mathbb{E}\{c_n[k, t]\}$ is computationally prohibitive due to the integral over the probability density function (PDF) of the fading channel. To circumvent this, we derive a tractable deterministic lower bound. The key results are illustrated in Fig. 4.

Lemma 1 (Explicit lower bound): The expected capacity $\mathbb{E}\{c_n[k, t]\}$ is lower bounded by

$$\mathbb{E}\{c_n[k, t]\} \geq \bar{c}_n[k, t] \triangleq \log_2(1 + \beta_n[k, t] \bar{\gamma}_n[k, t]), \quad (26)$$

where $\bar{\gamma}_n[k, t] = p_n[k, t] g_n[k, t] / \delta^2$ denotes the average received SNR, and $\beta_n[k, t] = e^{\psi(\kappa_n[k, t])} / \kappa_n[k, t]$ characterizes the capacity loss due to fading severity, where $\psi(\cdot)$ is the Digamma function. Moreover, the bound is tight in high-SNR or strong-LOS regime, i.e., $\mathbb{E}\{c_n[k, t]\} \rightarrow \bar{c}_n[k, t]$ as $\bar{\gamma}_n[k, t] \rightarrow \infty$ or $\kappa_n[k, t] \rightarrow \infty$.

Proof: See Appendix D. ■

The channel fading severity $\beta_n[k, t] \in (0, 1)$ ranges from 0 in deep fading regimes ($\kappa \rightarrow 0$) to 0.56 in Rayleigh fading ($\kappa \rightarrow 1$), and 1 in strong LOS conditions ($\kappa \rightarrow \infty$). In low-altitude networks, the channel is typically dominated by LOS components (i.e., $\kappa \geq 4$) [37], under which the proposed method is nearly tight, as illustrated in Fig. 4.

Leveraging Lemma 1, we replace the stochastic constraint in $\mathcal{P}3$ -2 with a tractable deterministic surrogate.

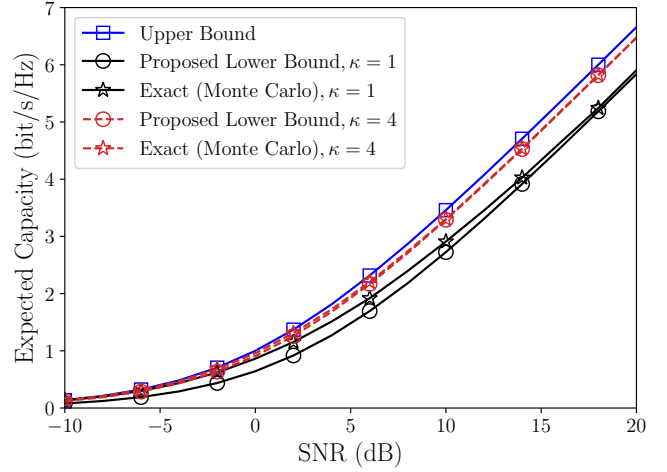


Fig. 4. Expected capacity vs. average SNR for different κ ($\kappa = 1$: Rayleigh, $\kappa = 4$: strong LOS). The common approximation yields a κ -invariant upper bound, whereas the proposed result gives a lower bound that becomes tight in the high-SNR or strong-LOS regime.

Consequently, the sum rate requirement is reformulated as:

$$\sum_{n \in \mathcal{N}, k \in \mathcal{K}, t \in \mathcal{T}_i} \bar{c}_n[k, t] a_n[k, t] \geq \bar{v}. \quad (27)$$

2) Convex Relaxation and Transformation: Firstly, we relax the binary RB allocation constraint such that $a_n[k, t] \in [0, 1]$. Then, to address the non-convexity inherent in the objective and rate-constrained resource allocation (specifically (27) derived from (23)), we employ a variable transformation strategy inspired by [15]. We introduce an auxiliary variable $\phi_n[k, t] = \bar{c}_n[k, t] a_n[k, t]$. Then, the transmission power variable is transformed to

$$p_n[k, t] = \begin{cases} \iota_n[k, t] \left(2^{\frac{\phi_n[k, t]}{a_n[k, t]}} - 1 \right), & a_n[k, t] > 0, \\ 0, & a_n[k, t] = 0, \end{cases} \quad (28)$$

where $\iota_n[k, t] = \delta^2 / (\beta_n[k, t] g_n[k, t])$ is a constant.

Substituting (28) into the energy consumption formula in (13), the objective function of $\mathcal{P}3$ -2 is reformulated as

$$\sum_{n \in \mathcal{N}, k \in \mathcal{K}, t \in \mathcal{T}_i} \iota_n[k, t] a_n[k, t] \left(2^{\frac{\phi_n[k, t]}{a_n[k, t]}} - 1 \right),$$

which is convex, as each summand is the perspective function of the convex function $f_1(x) = \iota_n[k, t] (2^x - 1)$ [38].

As a result, the original sum-rate constraint (27) becomes linear

$$\sum_{n \in \mathcal{N}, k \in \mathcal{K}, t \in \mathcal{T}_i} \phi_n[k, t] \geq \bar{v}.$$

Similarly, the power constraints $\sum_{n, k} p_n[k, t] \leq \bar{p}$ and $p_n[k, t] \geq 0$ are converted to

$$\sum_{n \in \mathcal{N}, k \in \mathcal{K}} \iota_n[k, t] a_n[k, t] \left(2^{\frac{\phi_n[k, t]}{a_n[k, t]}} - 1 \right) \leq \bar{p}, \quad \forall t \in \mathcal{T}_i,$$

and $\phi_n[k, t] \geq 0$, respectively.

By combining the deterministic lower bound, continuous relaxation, and variable transformation, $\mathcal{P}3$ -2 is

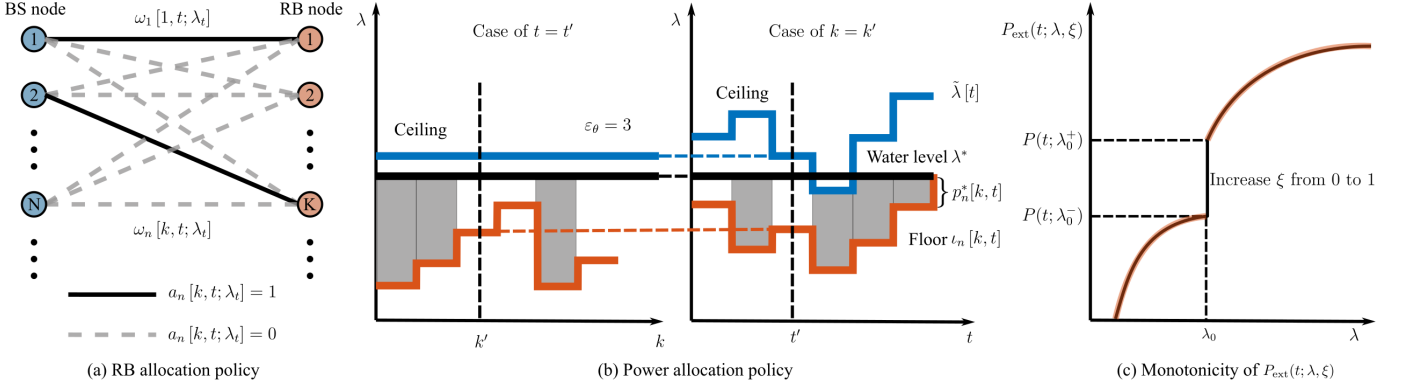


Fig. 5. Illustration of power and access control algorithm. (a) Optimal b-matching-based RB allocation: the left nodes represent BSs, the right nodes represent RB resources. The algorithm selects a minimum-weight matching under the constraint $\mathcal{A}(t)$. (b) Optimal power allocation via capped water-filling: the water level is capped by the per-slot sum-power limit. Since activation depends on the RB-allocation decision in (a), the RB (k, t) may remain inactive even if its floor lies below the water level. (c) P_{ext} increases monotonically with (λ, ξ) . The binary optimal solution exists for all λ (the same holds for $\Phi_{\text{ext}}(t; \lambda, \xi)$).

reformulated such that the objective function and all constraints become convex. The resulting relaxed problem is therefore convex, and its formulation is given as follows.

$$\mathcal{P}4: \text{minimize}_{\mathbf{A}_i, \Phi_i} \sum_{n \in \mathcal{N}, k \in \mathcal{K}, t \in \mathcal{T}_i} \iota_n[k, t] a_n[k, t] \left(2^{\frac{\phi_n[k, t]}{a_n[k, t]}} - 1 \right)$$

$$\text{s.t.} \quad \sum_{n \in \mathcal{N}, k \in \mathcal{K}, t \in \mathcal{T}_i} \phi_n[k, t] \geq \bar{v}, \quad (29)$$

$$\phi_n[k, t] \geq 0, \forall n \in \mathcal{N}, k \in \mathcal{K}, t \in \mathcal{T}_i, \quad (30)$$

$$\sum_{n \in \mathcal{N}, k \in \mathcal{K}} \iota_n[k, t] a_n[k, t] \left(2^{\frac{\phi_n[k, t]}{a_n[k, t]}} - 1 \right) \leq \bar{p}, \forall t \in \mathcal{T}_i, \quad (31)$$

$$\sum_{k \in \mathcal{K}} a_n[k, t] \leq \varepsilon_\theta, \forall n \in \mathcal{N}, t \in \mathcal{T}_i, \quad (32)$$

$$\sum_{n \in \mathcal{N}} a_n[k, t] \leq 1, \forall k \in \mathcal{K}, t \in \mathcal{T}_i, \quad (33)$$

$$a_n[k, t] \in [0, 1], \forall n \in \mathcal{N}, k \in \mathcal{K}, t \in \mathcal{T}_i, \quad (34)$$

where $\Phi_i \triangleq \{\phi_n[k, t]\}_{n \in \mathcal{N}, k \in \mathcal{K}, t \in \mathcal{T}_i}$.

3) Efficient and Binary-Enforcing Algorithm: One can apply commercial tools such as CVX [39] to solve $\mathcal{P}4$. However, these methods are computationally inefficient for high-dimensional problems. More importantly, they produce non-deterministic access decisions, since the obtained variables $a_n[k, t]$ are continuous rather than binary. We are therefore motivated to develop a specialized, efficient algorithm that enforces binary constraints. The main idea is to analyze the Karush-Kuhn-Tucker (KKT) conditions of the relaxed problem $\mathcal{P}4$ and exploit the resulting structure to retrieve the optimal binary solution.

The next proposition derives the optimal control for $\mathcal{P}4$ based on KKT analysis. It shows that the power allocation adheres to a capped water-filling rule, and the RB assignment becomes a linear program governed by the water level, as illustrated in Fig. 5.

Proposition 2 (Optimal resource allocation): There exists an optimal solution to $\mathcal{P}4$ such that for each $t \in \mathcal{T}_i$, the optimal RB allocation $\mathbf{A}[t; \lambda_t] \triangleq \{a_n[k, t; \lambda_t]\}_{n, k}$

belongs to the optimal solution set of the per-slot linear program

$$\mathcal{A}^*(t; \lambda_t) \triangleq \arg \min_{\mathbf{A}[t] \in \mathcal{A}(t)} \sum_{n \in \mathcal{N}, k \in \mathcal{K}} w_n[k, t; \lambda_t] a_n[k, t], \quad (35)$$

with weights

$$w_n[k, t; \lambda_t] = p_n[k, t; \lambda_t] - \ln 2 \lambda_t \bar{c}_n[k, t; \lambda_t],$$

where

$$\mathcal{A}(t) \triangleq \left\{ \{a_n[k, t]\}_{n, k} : (32)-(34) \right\}.$$

Here, the optimal power and capacity follow a capped water-filling structure

$$p_n[k, t; \lambda_t] = [\lambda_t - \iota_n[k, t]]^+, \quad (36)$$

$$\bar{c}_n[k, t; \lambda_t] = [\log_2(\lambda_t) - \log_2(\iota_n[k, t])]^+, \quad (37)$$

where $[x]^+ \triangleq \max(0, x)$ and the effective per-slot water level is capped as

$$\lambda_t = \min \left\{ \frac{\lambda^*}{\ln 2}, \tilde{\lambda}_t \right\}.$$

The per-slot capping level $\tilde{\lambda}_t$ is chosen to satisfy

$$P(t; \lambda) \triangleq \sum_{n \in \mathcal{N}, k \in \mathcal{K}} a_n[k, t; \lambda] [\lambda - \iota_n[k, t]]^+ = \bar{p}. \quad (38)$$

The global water level λ^* is determined by

$$\begin{aligned} \Phi(\lambda) &\triangleq \sum_{t \in \mathcal{T}_i} \Phi(t; \lambda) \\ &\triangleq \sum_{t \in \mathcal{T}_i} \sum_{n \in \mathcal{N}, k \in \mathcal{K}} a_n[k, t; \lambda_t] c_n[k, t; \lambda_t] = \bar{v}. \end{aligned} \quad (39)$$

Proof: See Appendix E. ■

As a result, Problem $\mathcal{P}4$ is reduced to solving equations (38) and (39). To address the potential non-uniqueness in $\mathcal{A}^*(t; \lambda_t)$, which may yield multi-valued and discontinuous functions $P(t; \lambda)$ and $\Phi(\lambda)$, we define the extended functions $P_{\text{ext}}(t; \lambda, \xi)$ and $\Phi_{\text{ext}}(\lambda, \xi)$ using a convex combination of extreme points. These extensions are shown to be optimal, continuous, and non-decreasing in Proposition 4.

Algorithm 1 Efficient power and access control.

Input: \bar{v} , ε_θ , $g_n[k, t]$ and $\kappa_n[k, t]$ for all n, k and $t \in \mathcal{T}_i$

- 1) Obtain $\tilde{\lambda}_t$ and $\tilde{\xi}_t$ by computing $P_{\text{ext}}(t; \lambda, \xi) = \bar{p}$ via bi-section search for all t .
- 2) Obtain λ^- and λ^+ with $\Phi_{\text{ext}}(\lambda_t^-, 0) \leq \bar{v} \leq \Phi_{\text{ext}}(\lambda_t^+, 0)$ via bi-section search.
- 3) Obtain ξ^* by computing $\Phi_{\text{ext}}(\lambda_t, \xi_t) = \bar{v}$ via bi-section search, with $\xi_t = \min\{\xi, \tilde{\xi}_t\}$.

Output: $p_n^*[k, t] \leftarrow p_n[k, t; \lambda_t]$, $a_n^*[k, t] \leftarrow a_n[k, t; \lambda_t^-, \xi^*]$, and $E^*(t_i, t_{i+1}) \leftarrow \sum_{t \in \mathcal{T}_i} P_{\text{ext}}(t; \lambda_t^-, \xi_t^*)$.

Additionally, the existence of a binary RB allocation solution for any λ is proven in Proposition 3, which enables the construction of a feasible binary policy.

Proposition 3 (Binary RB allocation): For any λ , there exists a solution $\mathbf{A}[t; \lambda_t] \in \mathcal{A}^*(t; \lambda)$ such that $a_n[k, t; \lambda] \in \{0, 1\}$ for all $n \in \mathcal{N}, k \in \mathcal{K}, t \in \mathcal{T}_i$.

Proof: See Appendix E. ■

As a result, Problem (35) can be solved by the b-matching algorithm. While Proposition 3 guarantees the existence of binary optimal solutions, the set $\mathcal{A}^*(t; \lambda_t^*)$ may contain multiple optimal RB allocations at certain critical water levels.

Let λ_0 denote such a critical point. We define two limiting binary solutions $\mathbf{A}^-[t; \lambda_0] \triangleq \lim_{\lambda \rightarrow \lambda_0^-} \mathbf{A}[t; \lambda]$ and $\mathbf{A}^+[t; \lambda_0] \triangleq \lim_{\lambda \rightarrow \lambda_0^+} \mathbf{A}[t; \lambda]$, which always exist according to Proposition 3. For any $\xi \in [0, 1]$, we construct the convexified RB allocation as $\mathbf{A}[t; \lambda_0, \xi] = (1 - \xi)\mathbf{A}^-[t; \lambda_0] + \xi\mathbf{A}^+[t; \lambda_0]$. Accordingly, the extended per-slot power and sum rate are defined, respectively, as

$$P_{\text{ext}}(t; \lambda, \xi) = \sum_{n \in \mathcal{N}, k \in \mathcal{K}} a_n[k, t; \lambda, \xi] [\lambda - \iota_n[k, t]]^+,$$

$$\Phi_{\text{ext}}(t; \lambda, \xi) = \sum_{n \in \mathcal{N}, k \in \mathcal{K}} a_n[k, t; \lambda, \xi] c_n[k, t; \lambda_t].$$

Proposition 4 (Properties of extended functions): Define the extended domain $\mathcal{D} \triangleq \{(\lambda, \xi) : \lambda \in \mathbb{R}_{0+}, \xi \in [0, 1]\}$. Then, the following properties hold for $P_{\text{ext}}(t; \lambda, \xi)$ (similar conditions hold for $\Phi_{\text{ext}}(t; \lambda, \xi)$).

1. **Optimality:** $\mathbf{A}[t; \lambda, \xi] \in \mathcal{A}^*(t; \lambda)$ for all $\xi \in [0, 1]$; and $P_{\text{ext}}(t; \lambda, \xi) = (1 - \xi)P(t; \lambda^-) + \xi P(t; \lambda^+)$.

2. **Continuity:** The extended functions are continuous with respect to $\xi \in [0, 1]$. Furthermore, at any point λ_0 where discontinuity occurs in λ , the boundaries satisfy

$$\lim_{\lambda \rightarrow \lambda_0^-} P_{\text{ext}}(t; \lambda, \xi) = P_{\text{ext}}(t; \lambda_0, 0),$$

$$\lim_{\lambda \rightarrow \lambda_0^+} P_{\text{ext}}(t; \lambda, \xi) = P_{\text{ext}}(t; \lambda_0, 1).$$

3. **Monotonicity:** $P_{\text{ext}}(t; \lambda_1, \xi_1) \leq P_{\text{ext}}(t; \lambda_2, \xi_2)$ if $\lambda_1 \leq \lambda_2$ for any ξ_1 and ξ_2 ; and $P_{\text{ext}}(t; \lambda, \xi_1) \leq P_{\text{ext}}(t; \lambda, \xi_2)$ if $\xi_1 \leq \xi_2$ for any λ .

Proof: See Appendix E. ■

Proposition 4 establish three key results: continuity ensures the existence of a solution to equations (38) and

Algorithm 2 Graph-based sampling timing control.

Input: θ , $g_n[k, t]$ and $\kappa_n[k, t]$ for all n, k, t

- 1) Construct the graph \mathcal{G} based on Fig. 6. Compute the weights by solving $\mathcal{P}3$ -2 using Algorithm 1.
- 2) Find the optimal sampling time sequence \mathbf{t}^* using the shortest-path algorithm on the graph \mathcal{G} .

Output: \mathcal{A}^* , \mathcal{P}^* , \mathbf{t}^* , and $E^*(\theta)$

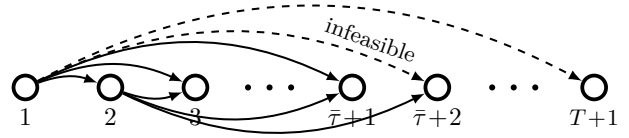


Fig. 6. Construction of the timing-control graph. Each vertex represents a sampling instant, and each directed edge denotes a communication interval. The weight of each feasible edge is obtained by solving the inner optimization problem associated with its endpoints.

(39); monotonicity allows for efficient bisection-searching algorithmic design; and optimality confirms that the found solution is optimal.

Building on the results in Propositions 2–4, we propose a power and access control algorithm (Algorithm 1), which determines the optimal solution to the relaxed Problem $\mathcal{P}4$ by effectively solving the equations $P_{\text{ext}}(t; \lambda, \xi) = \bar{p}$ for all t and $\Phi_{\text{ext}}(\lambda_t, \xi_t) \triangleq \sum_t \Phi_{\text{ext}}(t; \lambda_t, \xi_t) = \bar{v}$. The procedure executes a two-stage iterative search: it first computes the local capping thresholds $\tilde{\lambda}_t$ and combining parameters $\tilde{\xi}_t$, followed by the determination of the global water-level λ^* and instantaneous ξ_t^* . For ensuring the binary of RB allocation, one can simply choose the policy based on λ_t^+ and the energy consumption is $\sum_{t \in \mathcal{T}_i} P_{\text{ext}}(t; \lambda_t^+, 0)$.

B. Outer Solution: Sampling Timing Control

This section addresses $\mathcal{P}3$ -1 by transforming it into a shortest path problem on a weighted directed acyclic graph.

1) **Graph Construction:** We first construct a timing-control graph $\mathcal{G} = \{\mathbf{v}, \mathbf{e}, \mathbf{w}\}$, as depicted in Fig. 6. The vertex set $\mathbf{v} = \{1, \dots, T+1\}$ represents the discrete time indices of all possible sampling instants. The terminal node $T+1$ is introduced to mark the boundary of the optimization horizon, ensuring the final transmission interval is accounted for. The directed edge set $\mathbf{e} = \{(v_i, v_j)\}$ represents valid transmission intervals. An edge exists from node i to node j (where $v_i, v_j \in \mathbf{v}$) if and only if the interval duration satisfies the AoI constraint, i.e., $1 \leq t_i - t_j \leq \bar{\tau}$. The weight set $\mathbf{w} = \{w_{i,j}\}$ assigns a cost to each edge, defined as the minimum energy consumption required for complete data delivery over the interval $[t_i, t_{i+1}) \cap \mathbb{Z}_+$. Specifically, $w_{i,j} = E^*(t_i, t_j)$, which is obtained by solving the inner problem $\mathcal{P}3$ -2.

2) **Graph Equivalence:** By construction, any feasible sampling sequence $\mathbf{t} = \{1 = t_0 < t_1 < \dots < t_{T+1} = T+1\}$ maps bijectively to a directed path $1 \rightarrow t_1 \rightarrow \dots \rightarrow t_{T+1} = T+1$ in \mathcal{G} . Each edge (t_i, t_j) in \mathcal{G} satisfies

the AoI constraint $1 \leq t_j - t_i \leq \bar{\tau}$, as shown in Fig. 6. Thus, any path from node 1 to node $T + 1$ represents a sampling sequence that satisfies $t_0 = 1$, $t_{T+1} = T + 1$, and $t_k \in \mathcal{T}, \forall k$. Conversely, any feasible solution in Υ constitutes a valid path from node 0 to node $T + 1$ in \mathcal{G} , and vice versa.

The weight of each feasible edge (t_i, t_{i+1}) is defined as $w_{i,i+1} = E^*(t_i, t_{i+1})$. The total length of a path is $\sum_i w_{i,i+1}$, which equals the objective function $\sum_i E^*(t_i, t_{i+1})$. Hence, $\mathcal{P}3$ -1 is equivalent to a graph shortest-path problem. This equivalence is formalized in the following proposition.

Proposition 5 (Equivalence of $\mathcal{P}3$ -1): Finding the optimal sampling sequence \mathbf{t}^* for $\mathcal{P}3$ -1 is equivalent to finding the shortest path from node 1 to node $T + 1$ in \mathcal{G} .

3) Graph-Based Algorithm: As a result, Problem $\mathcal{P}3$ -1 is equivalent to a shortest path problem on a weighted directed graph. The graph-based algorithm is summarized in Algorithm 2. It proceeds in two phases: (i) construct the timing-control graph \mathcal{G} with edge weights given by the optimal interval energy $E^*(\cdot, \cdot)$; and (ii) find the shortest path from node 1 to node $T + 1$.

C. Optimality and Complexity Analysis

Overall, Algorithm 2 yields an asymptotically optimal joint timing, power, and access control policy in the high-SNR or strong-LOS regime, with complexity $\mathcal{O}(\bar{\tau}^2 NK^2 T \log(\epsilon^{-1}))$. Hence, the resulting Pareto frontier of $\mathcal{P}1$ is asymptotically optimal and can be obtained with overall complexity $\mathcal{O}(\bar{\tau}^2 NK^3 T \log(\epsilon^{-1}))$. The detailed analysis is as follows.

1) Optimality: The optimality of Algorithm 1 is guaranteed because its output satisfies the KKT conditions established in Proposition 2. The only approximation gap arises from the lower bound of the expected sum rate. The asymptotic tightness of this bound is established in Lemma 1, implying that Algorithm 1 achieves asymptotic optimality in the high-SNR or strong-LOS regime. Moreover, since the graph search for timing control is globally optimal by Proposition 5, Algorithm 2 also achieves asymptotic optimality in the high-SNR or strong-LOS regime.

2) Complexity: The computational complexity of Algorithm 1 is dominated by the weighted bipartite matching subroutine (successive shortest path [40]) executed within the bisection search over T time slots. With the matching complexity of $\mathcal{O}(NK^2 + (NK + K^2) \log(N + K)) \approx \mathcal{O}(NK^2)$ and a bisection accuracy of $\mathcal{O}(\log(\epsilon^{-1}))$, the total complexity of Algorithm 1 is $\mathcal{O}(NK^2 T \log(\epsilon^{-1}))$.

Then we analyze the complexity of Algorithm 2. To analyze the complexity of constructing the graph \mathcal{G} , we partition the edges into $\bar{\tau}$ groups indexed by $c \in 1, \dots, \bar{\tau}$. In group c , every edge (v_i, v_j) induces a transmission interval of length c ; that is, $v_j - v_i = c$, as depicted in Fig. 7. Since any feasible edge in \mathcal{G} must satisfy $1 \leq t_i - t_j \leq \bar{\tau}$, all these $\bar{\tau}$ groups collectively constitutes the complete edge set of \mathcal{G} .

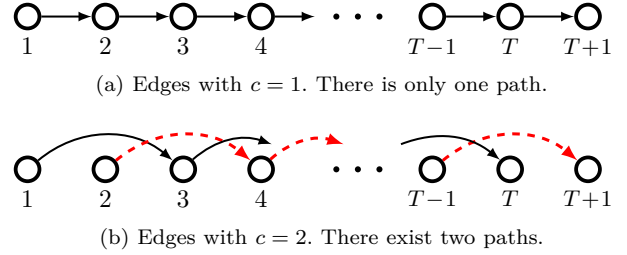


Fig. 7. Illustration of edge division based on communication interval c .

For each group c , there are c paths from near 1 to near $T + 1$, and the cost for calculating the weight of edges in this group is bounded by $cNK^2 T \log(\epsilon^{-1})$. For example, when $c = 1$, there is only one path $1 \rightarrow 2 \rightarrow 3 \rightarrow \dots \rightarrow T + 1$. Therefore, the complexity is

$$\sum_{i=1}^T NK^2 \log(\epsilon^{-1}) (t_{i+1} - t_i) = NK^2 T \log(\epsilon^{-1}).$$

When $c = 2$, there are only two possible paths $1 \rightarrow 3 \rightarrow 5 \rightarrow \dots \rightarrow T$ and $2 \rightarrow 4 \rightarrow 6 \rightarrow \dots \rightarrow T + 1$, and the communication interval is 2. Therefore, the complexity is

$$2 \sum_{i=1}^{\lfloor T/2 \rfloor} NK^2 \log(\epsilon^{-1}) (t_{i+1} - t_i) \leq 2NK^2 T \log(\epsilon^{-1}).$$

Following the same reasoning, the complexity for groups with $c \in \{3, \dots, \bar{\tau}\}$ can be derived analogously.

Hence, the complexity of graph construction is bounded by

$$\sum_{c=1}^{\bar{\tau}} cNK^2 T \log(\epsilon^{-1}) = \frac{(\bar{\tau} + 1)\bar{\tau}}{2} NK^2 T \log(\epsilon^{-1})$$

which is the order of $\mathcal{O}(\bar{\tau}^2 NK^2 T \log(\epsilon^{-1}))$.

Finally, recall that the Pareto frontier is computed over θ values. The overall complexity is $\mathcal{O}(\bar{\tau}^2 NK^3 T \log(\epsilon^{-1}))$.

V. Extension to Problem Variants

Problem $\mathcal{P}1$ is adopted as a canonical formulation. In practice, one may encounter a broad class of variants, such that objective transformations and single-objective specializations. We next discuss three representative variants and specify conditions under which our approach remains applicable.

A. Objective Transformation

To represent heterogeneous requirements, we introduce a generic objective vector

$$\mathbf{g}(\theta, E) = (g_1(\theta), g_2(E))^T : \mathbb{R}^2 \rightarrow \mathbb{R}^2,$$

where $g_1(\theta) : \mathbb{R} \rightarrow \mathbb{R}$ penalizes the spatiotemporal load cap θ , and $g_2(E) : \mathbb{R} \rightarrow \mathbb{R}$ penalizes the UAV energy consumption E . The resulting nonlinear transformed bi-objective problem is formulated as

$$\mathcal{P}_1^{\forall} : \min_{\boldsymbol{\pi} \in \Pi} \{g_1(\theta(\boldsymbol{\pi})), g_2(E(\boldsymbol{\pi}))\}, \text{ s.t. } \tau[t] \leq \bar{\tau}, \forall t \in \mathcal{T}.$$

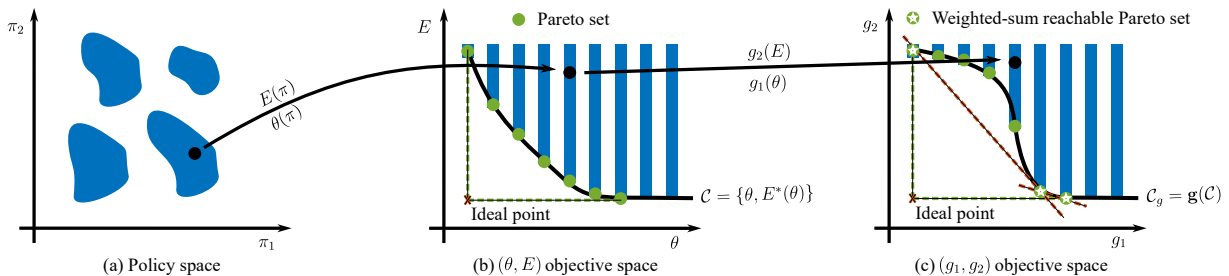


Fig. 8. Illustration of Pareto optimality for a two-variable, two-objective optimization problem example. (a) The nonconvex policy space. (b) Bi-objective (E, θ) space, where the feasible space and the objective space are non-convex and non-continuous, thereby classical heuristic algorithms are challenging to find the complete Pareto frontier. (c) Bi-objective (g_2, g_1) space, where the Pareto frontier is non-concave, thereby, the weighting method cannot guarantee the discovery of all Pareto optima. Conversely, one can map a point on the transformed Pareto frontier back to the original frontier and then to the policy space, thereby obtaining an optimal policy for the corresponding variant problems.

Some practical choices of transformation functions include (i) linear models for constant marginal costs [41], (ii) barrier-type metrics for delay-sensitive congestion [42], and (iii) non-convex logistic forms representing saturation or risk thresholds [43], [44].

Let \mathcal{C} denote the Pareto frontier of the original Problem \mathcal{P}_1 , and let \mathcal{C}_g denote the Pareto frontier of the transformed Problem \mathcal{P}_1^v . The following theorem establishes that, under the mild assumption that $\mathbf{g}(\cdot) = (g_1(\cdot), g_2(\cdot))$ is component-wise strictly increasing, the Pareto frontier of \mathcal{P}_1^v can be readily obtained without resolving the optimization problem.

Theorem 2 (Order-preserving equivalence): If $\mathbf{g}(\cdot) = (g_1(\cdot), g_2(\cdot))$ is component-wise strictly increasing over the feasible ranges of θ and E , then \mathcal{P}_1^v and \mathcal{P}_1 share the same set of Pareto-optimal policies, and

$$\mathcal{C}_g = \mathbf{g}(\mathcal{C}) \triangleq \{(g_1(\theta), g_2(E)) : (\theta, E) \in \mathcal{C}\}.$$

Proof: See Appendix B. ■

B. Preference-based Scalarization

For preset user preferences, the bi-objective Pareto optimization reduces to a single-objective problem. Let $u : \mathbb{R}^2 \rightarrow \mathbb{R}$ be a nonlinear increasing function that aggregates the objective vector (θ, E) into a single measure. The resulting scalarized optimization problem is formulated as

$$\mathcal{P}_2^v : \min_{\pi \in \Pi} u(\mathbf{g}(\theta(\pi), E(\pi))), \text{ s.t. } \tau[t] \leq \bar{\tau}, \forall t \in \mathcal{T}.$$

The relationship between the optimal solution of this scalarized problem and the Pareto frontier of the original multi-objective problem is established in the following.

Theorem 3 (Sufficiency of monotone utility [36, Theorem 2.6.2]): If the value function $u(\cdot)$ is strongly increasing, i.e., for any $\mathbf{x}, \mathbf{y} \in \mathbb{R}^2$ with $\mathbf{x} \preceq \mathbf{y}$, it holds that $u(\mathbf{x}) < u(\mathbf{y})$, then any solution to \mathcal{P}_2^v lies in the Pareto frontier of \mathcal{P}_1 .

A canonical example satisfying this monotonicity condition is the weighted L_p metric, defined as

$$u = (\alpha |\theta - \theta'|^p + (1 - \alpha) |E - E'|^p)^{1/p}, \alpha \in [0, 1], p \geq 1.$$

Here, the weight α explicitly quantifies the trade-off preference between the load penalty and energy consumption,

and (θ', E') is a special target. The metric becomes a weighted-sum metric when $p = 1$ and $\theta' = E' = 0$.

C. Budget-Constrained Optimization

This formulation focuses on a single primary objective while treating the secondary objective as a constraint (referred to as the ε -constraint method). When the energy consumption is the primary concern, the goal is to minimize the energy cost E or $g_2(E)$ subject to an admissible upper bound ε_θ on the spatiotemporal load

$$\mathcal{P}_v^3 : \min_{\pi \in \Pi} g_2(E(\pi)), \text{ s.t. } \tau[t] \leq \bar{\tau}, \forall t \text{ and } g_1(\theta(\pi)) \leq \varepsilon_\theta.$$

Similarly, one can formulate a load-cap minimization problem with an energy constraint.

Theorem 4 (Sufficiency of partial optimization [36, Theorem 2.10.3]): Any optimal solution to \mathcal{P}_v^3 (where the constraint is active) is Pareto optimal for the original problem \mathcal{P}_1 .

The established theorems provide a transfer rule for system optimization, as illustrated in Fig. 8. Once the Pareto frontier \mathcal{C} of \mathcal{P}_1 is computed, the solutions for the transformed-objective problem \mathcal{P}_v^1 , the preference-based single-objective formulation \mathcal{P}_v^2 , and the budget-constrained single-objective formulation \mathcal{P}_v^3 can be obtained through direct mapping or by searching over the frontier \mathcal{C} . In other words, we can recover the solutions to these variants without re-solving the problems. This offers two main benefits. First, we bypass the analytical and computational difficulties of directly solving the variants. When the variants are non-convex or intractable, these transfer rules enable efficient recovery of the optimal solutions. Second, it shows strong potential for emergency response and policy adaptation in safety-critical applications.

VI. Simulation Results

We consider a UAV-based patrol system, where a UAV follows a circular trajectory to monitor a $200 \times 200 m^2$ area. The UAV operates at an altitude of 50 m with a flight speed of 6 m/s. On the ground, N BSs are deployed, with their positions randomly generated.

TABLE I
Default Implementation Parameters

Parameter	Description
Patrol UAV trajectory	Circular trajectory at 50 m altitude.
UAV speed	Uniform in 6 m/s.
Base station location	Uniformly distributed at ground level (0 m).
Carrier frequency	$f_c = 3$ GHz.
Bandwidth	$B = 10$ MHz.
Noise power	$\sigma^2 = -90$ dBm.
Path loss (LOS)	$22.0 + 28.0 \log_{10}(d) + 20 \log_{10}(f_c)$.
Path loss (NLOS)	$22.7 + 36.7 \log_{10}(d) + 26 \log_{10}(f_c)$.
LOS probability	$\mathbb{P}(\text{LOS}, \theta) = (1 + 6 \times \exp(-0.15[\theta - 6]))^{-1}$, where θ is elevation angle.
Shadowing	Log-normal distribution with 0 dB mean, 8 dB variance, and 5 m correlation distance.

The channel gain is realized by $h_n[k, t] = g_n[k, t] \xi_n[k, t]$ according to (1). Specifically, the shape parameters $\kappa_n[k, t]$ of Gamma distribution of small-scale fading $\xi_n[k, t]$ are set randomly in $[1, 30]$. Same as [16], the large-scale fading $g_n[k, t]$ includes path loss and shadowing, where the path loss is generated by 3GPP Urban Micro (UMi) model [45] and the channel block state is generated by LOS probability model [46], while the shadowing is modeled by a log-normal distribution, with zero mean and a variance of 8, and a correlation distance of 5 m. The default implementation parameters are listed in Table I.

A. Performance on Power and Access Control

Fig. 9 illustrates the performance of the power and access control algorithm in Algorithm 1 based on 100 repeated random simulations, including computational complexity, optimality, and feasibility. As a benchmark, CVX [39] is used to solve the relaxed problem $\mathcal{P}4$; hence, its objective value serves as a lower bound.

Fig. 9a compares the computational complexity. For practical evaluation, only cases with running time below 100 s are reported for the CVX-based baseline. The proposed algorithm exhibits an empirical slope of approximately 1.3, indicating a runtime scaling of about $\mathcal{O}(K^{1.3})$ over the tested regime, which is below the theoretical upper bound $\mathcal{O}(K^2)$. Across the tested range, the proposed algorithm is more than 200 times faster than the CVX-based baseline and the speedup increases with the number of RBs, highlighting the suitability of the proposed method for practical implementation.

Fig. 9b shows that the curves produced by the proposed algorithm and the CVX-based baseline overlap across all tested settings, indicating that the proposed solution closely matches the lower bound and is thus near-optimal. Moreover, the proposed algorithm always returns binary RB allocations and therefore remains feasible for all cases, as shown in Fig. 9c. In contrast, the relaxed CVX solution increasingly violates the binary constraints as the number of RBs grows, with the violation ratio reaching 50% when $K = 150$.

B. Performance on Sampling Timing Control

We compare the age-aware sampling scheme with the following three baselines (all use the proposed optimal power and access control).

- Instantaneous rate [4]: Trade-off spatiotemporal load cap and energy efficiency under the piecewise rate constraint, i.e., $c_m(t) \geq S/\bar{\tau}, \forall t$.
- Average rate [5]: Trade-off spatiotemporal load cap and energy efficiency under the average rate constraint, i.e., $\sum_t c_m(t)/T \geq S/\bar{\tau}$.
- Periodic sampling: The sampling time is fixed as $t_k = (k-1)\bar{\tau}$, while the resource allocation strategy follows the proposed schemes.

Fig. 10a illustrates the Pareto frontiers achieved by these schemes. It is observed that the non-predictive scheme (instantaneous rate) is significantly suboptimal, by more than 20 dB compared with the other three predictive schemes. This highlights the efficiency of the proposed MPCComm framework. Although both the Periodic and proposed age-aware schemes exploit predictive information, the latter achieves substantial performance improvement by adaptively controlling the sampling instants. For example, given an energy budget of $E = 10$ dBm, the Periodic sampling method requires approximately 300 RBs to complete the task. In contrast, the proposed status-aware method needs only about 50 RBs.

Fig. 10b illustrates the fulfillment of the aerial timeliness requirement. First, although the average-rate method exhibits superior energy efficiency and RB utilization compared with other baselines, it fails to satisfy the AoI requirement. This is because it optimizes the long-term average sum rate rather than per-interval performance; thus, intervals with poor channel conditions remain underserved, leading to unstable AoI satisfaction even as θ increases. The instantaneous-rate method shows clear disadvantages, as it consumes the most resources while still failing to meet the peak AoI constraint. In contrast, the proposed predictive age-aware scheme satisfies the AoI constraint across all cases.

Fig. 10c evaluates the stability of RB utilization for fixed average energy. The proposed algorithm achieves stable RB utilization by explicitly controlling the sampling timing, and this stability is maintained even under dynamic conditions. This behavior supports the reliability of the proposed design over long-term operation. In contrast, without sampling control, the RB utilization increases over time and eventually saturates at the maximum budget when $T > 200$ s.

VII. Conclusion

In this paper, we propose an MPCComm-based strategy for timely status updates in low-altitude networks. We formulate a bi-objective optimization problem to balance energy consumption and terrestrial channel occupation, subject to a data freshness constraint. We characterize the Pareto frontier using the ϵ -constraint method and

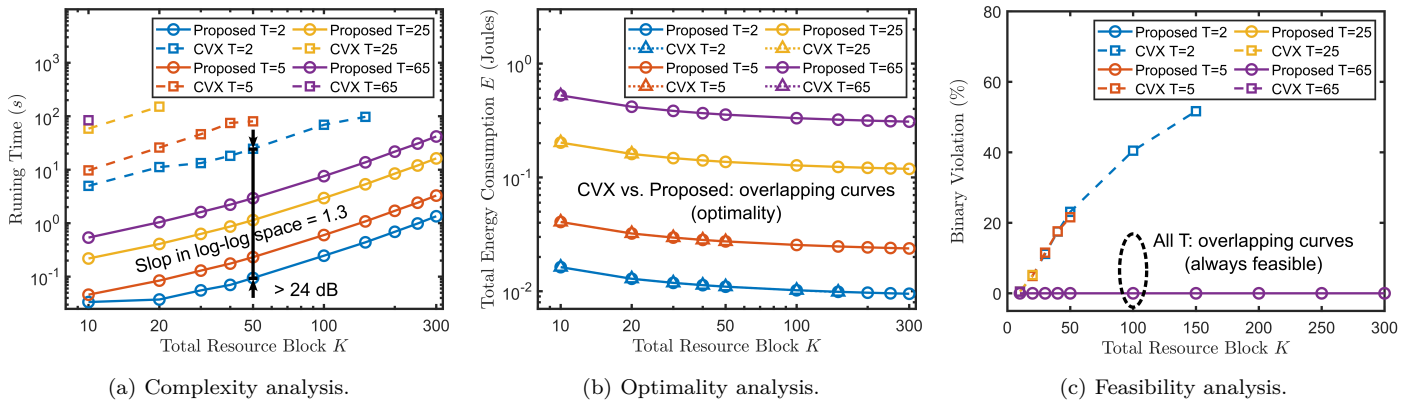


Fig. 9. Complexity, feasibility, and optimality of Algorithm 1 versus K and T for $N = 5$.

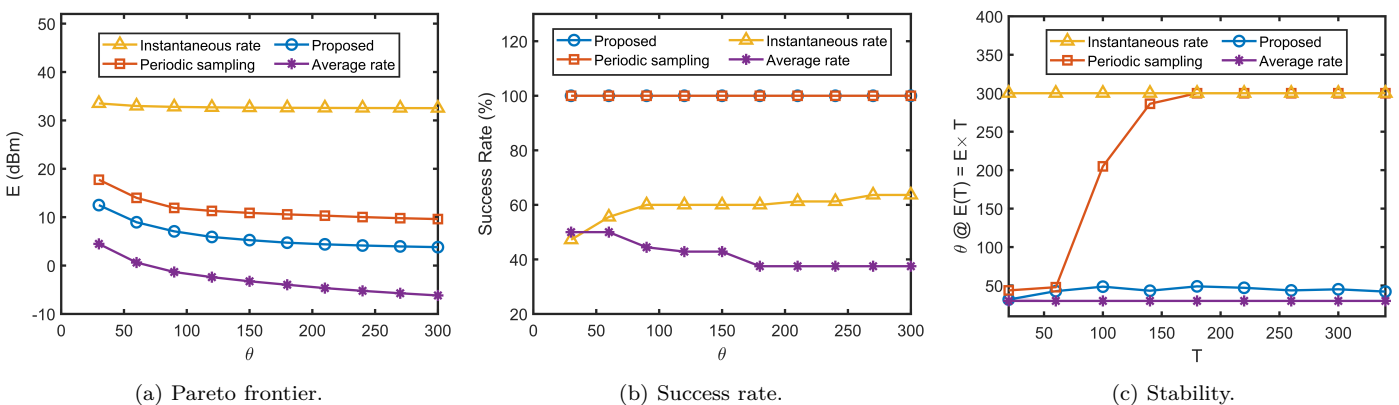


Fig. 10. Pareto frontier, success rate, and stability analysis for Algorithm 2 with $N = 5$.

develop a graph-based algorithm consisting of a low-complexity power and access control layer and an age-aware sampling control layer. The algorithm is asymptotically optimal, with a theoretical worst-case complexity of $\mathcal{O}(\bar{\tau}^2 N K^3 T \log(\epsilon^{-1}))$, and that its empirical complexity scales as $\mathcal{O}(\bar{\tau}^2 N K^{2.3} T \log(\epsilon^{-1}))$. Moreover, the proposed approach is applicable to a broad class of problem variants, including objective transformations and single-objective specializations. Numerical results show that our approach achieves up to a sixfold reduction in RB usage and a 6 dB energy saving compared to several benchmark schemes.

References

- [1] Q. Wu, J. Xu, Y. Zeng, D. W. K. Ng, N. Al-Dhahir, R. Schober, and A. L. Swindlehurst, "A comprehensive overview on 5G-and-beyond networks with UAVs: From communications to sensing and intelligence," *IEEE J. Sel. Areas Commun.*, vol. 39, no. 10, pp. 2912–2945, 2021.
- [2] M. Song, Y. Lin, J. Wang, G. Sun, C. Dong, N. Ma, D. Niyato, and P. Zhang, "Trustworthy intelligent networks for low-altitude economy," *IEEE Commun. Mag.*, vol. 63, no. 7, pp. 72–79, 2025.
- [3] A. S. Abdalla and V. Marojevic, "Next generation intelligent low-altitude economy deployments: The O-RAN perspective," *IEEE Wireless Commun.*, vol. 33, no. 1, pp. 20–28, 2026.
- [4] A. S. Matar and X. Shen, "Joint optimization of user association, power control, and dynamic spectrum sharing for integrated aerial-terrestrial network," *IEEE J. Sel. Areas Commun.*, vol. 43, no. 1, pp. 396–409, 2025.
- [5] H. Zhang, B. Li, Y. Rong, Y. Zeng, and R. Zhang, "Joint optimization of transmit power and trajectory for UAV-enabled data collection with dynamic constraints," *IEEE Trans. Commun.*, pp. 1–1, 2025.
- [6] S. Kaul, R. Yates, and M. Gruteser, "Real-time status: How often should one update?" in *Proc. IEEE INFOCOM*, 2012, pp. 2731–2735.
- [7] J. Luo and N. Pappas, "On the cost of consecutive estimation error: Significance-aware non-linear aging," *IEEE Trans. Inf. Theory*, vol. 71, no. 10, pp. 7976–7989, 2025.
- [8] J. Luo and N. Pappas, "On the role of age and semantics of information in remote estimation of Markov sources," *IEEE Trans. Commun.*, vol. 74, Apr. 2026.
- [9] J. Luo, E. Delfani, M. Salimnejad, and N. Pappas, "From information freshness to semantics of information and goal-oriented communications," *arXiv preprint arXiv:2512.12758*, 2025.
- [10] J. Chen, B. Li, H. Sun, S. Cui, and N. Pappas, "Predictive communications for low-altitude networks," *IEEE Internet Things Mag.*, pp. 1–8, 2026.
- [11] X. He, L. Li, Y. Mo, J. Huang, and S. J. Qin, "A distributed route network planning method with congestion pricing for drone delivery services in cities," *Transp. Res. Part C Emerg. Technol.*, vol. 160, p. 104536, 2024.
- [12] Y. Zeng, J. Chen, J. Xu, D. Wu, X. Xu, S. Jin, X. Gao, D. Gesbert, S. Cui, and R. Zhang, "A tutorial on environment-aware communications via channel knowledge map for 6G," *IEEE Commun. Surveys Tuts.*, pp. 1–1, 2024.
- [13] H. Wang, J. Zhang, G. Nie, L. Yu, Z. Yuan, T. Li, J. Wang, and G. Liu, "Digital twin channel for 6G: Concepts, architectures and potential applications," *IEEE Commun. Mag.*, vol. 63, no. 3, pp. 24–30, 2025.
- [14] B. Li, H. Zhang, M. Jia, J. Chen, and N. Pappas, "Joint

- CFO-channel estimation over CFO-coherent SS burst sets for low-altitude radio mapping,” 2025. [Online]. Available: <https://arxiv.org/abs/2512.01386>
- [15] B. Li and J. Chen, “Large timescale optimization for communications over aerial ad hoc networks with predetermined trajectories,” *IEEE Trans. Commun.*, vol. 72, no. 10, pp. 6371–6385, 2024.
- [16] B. Li and J. Chen, “Radio map-assisted approach for interference-aware predictive UAV communications,” *IEEE Trans. Wireless Commun.*, vol. 23, no. 11, pp. 16 725–16 741, 2024.
- [17] Z. Li, C. Su, Z. Su, H. Peng, Y. Wang, W. Chen, and Q. Wu, “Model predictive control enabled UAV trajectory optimization and secure resource allocation,” *IEEE Trans. Commun.*, vol. 73, no. 11, pp. 12 652–12 665, 2025.
- [18] R. Du, Z. Wei, Z. Yang, L. Yang, Y. Zeng, D. W. K. Ng, and J. Yuan, “Channel knowledge map-assisted dual-domain tracking and predictive beamforming for high-mobility wireless networks,” *IEEE Trans. Wireless Commun.*, vol. 25, pp. 10 968–10 985, 2026.
- [19] J. Li, Y. Chen, F. Liu, and J. Xu, “Channel knowledge map enabled low-altitude ISAC networks: Joint air corridor planning and base station deployment,” *IEEE Wireless Commun. Lett.*, vol. 15, pp. 975–979, 2026.
- [20] B. Li and J. Chen, “Radio map-assisted routing and predictive resource allocation over dynamic low-altitude networks,” *IEEE Trans. Wireless Commun.*, vol. 25, pp. 9955–9970, 2026.
- [21] W. Mei and R. Zhang, “Aerial-ground interference mitigation for cellular-connected UAV,” *IEEE Wireless Commun.*, vol. 28, no. 1, pp. 167–173, 2021.
- [22] M. Vaezi, X. Lin, H. Zhang, W. Saad, and H. V. Poor, “Deep reinforcement learning for interference management in UAV-based 3D networks: Potentials and challenges,” *IEEE Commun. Mag.*, vol. 62, no. 2, pp. 134–140, 2024.
- [23] H. Hu, K. Xiong, G. Qu, Q. Ni, P. Fan, and K. B. Letaief, “AoI-minimal trajectory planning and data collection in UAV-assisted wireless powered IoT networks,” *IEEE Internet Things J.*, vol. 8, no. 2, pp. 1211–1223, 2021.
- [24] J. Liu, P. Tong, X. Wang, B. Bai, and H. Dai, “UAV-aided data collection for information freshness in wireless sensor networks,” *IEEE Trans. Wireless Commun.*, vol. 20, no. 4, pp. 2368–2382, 2021.
- [25] Z. Qin, Z. Wei, Y. Qu, F. Zhou, H. Wang, D. W. K. Ng, and C.-B. Chae, “AoI-aware scheduling for air-ground collaborative mobile edge computing,” *IEEE Trans. Wireless Commun.*, vol. 22, no. 5, pp. 2989–3005, 2023.
- [26] W. Yuan, S. Chen, H. He, Y. Hou, S. Chen, X. Tan, and J. Yang, “Hierarchical reinforcement learning-based joint trajectory planning and resource allocation in UAV-assisted IoT-sensor networks,” *IEEE Trans. Commun.*, vol. 73, no. 12, pp. 14 517–14 533, 2025.
- [27] J. Tang, J. Liu, X. He, L. Xie, L. Qu, and H. Dai, “Deep reinforcement learning for AoI-aware trajectory and phase-shift design in IRS-assisted UAV data collection,” *IEEE Trans. Wireless Commun.*, vol. 24, no. 12, pp. 10 613–10 628, 2025.
- [28] Z. Lu, Q. Wu, Z. Jia, C. Fei, J. Zhang, F. Zhou, and K.-K. Wong, “Joint trajectory planning and channel selection for AoI minimization in multi-UAV-assisted IoT networks,” *IEEE Trans. Wireless Commun.*, vol. 25, pp. 11 161–11 175, 2026.
- [29] A. M. Girgis, J. Park, M. Bennis, and M. Debbah, “Predictive control and communication co-design via two-way gaussian process regression and AoI-aware scheduling,” *IEEE Trans. Commun.*, vol. 69, no. 10, pp. 7077–7093, 2021.
- [30] M. Song, H. Shan, Y. Cheng, W. Zhuang, X. Li, Q. Zhang, and X. He, “On the spatio-temporal analysis and optimization of AoI in cell-free IIoT networks,” *IEEE Trans. Wireless Commun.*, vol. 23, no. 11, pp. 16 421–16 436, 2024.
- [31] F. Zhao, N. Pappas, M. Zhang, and H. H. Yang, “Age of information in random access networks with energy harvesting,” *IEEE J. Sel. Areas Commun.*, vol. 43, no. 11, pp. 3813–3829, 2025.
- [32] S. Mu, Y. Lu, R. Jiang, W. Chen, B. Ai, and D. Niyato, “AoI-aware online transmission optimization for wbans with unreliable information delivery,” *IEEE Trans. Wireless Commun.*, vol. 25, pp. 5622–5639, 2026.
- [33] M. Nakagami, “The m-distribution: A general formula of intensity distribution of rapid fading,” in *Statistical Methods in Radio Wave Propagation*, W. HOFFMAN, Ed. Pergamon, 1960, pp. 3–36.
- [34] H. Lu and Y. Zeng, “Delay-Doppler alignment modulation for spatially sparse massive MIMO communication,” *IEEE Trans. Wireless Commun.*, vol. 23, no. 6, pp. 6000–6014, 2024.
- [35] M. Salimnejad, M. Kountouris, and N. Pappas, “Real-time reconstruction of markov sources and remote actuation over wireless channels,” *IEEE Trans. Commun.*, vol. 72, no. 5, pp. 2701–2715, 2024.
- [36] K. Miettinen, *Nonlinear Multiobjective Optimization*, 1st ed., ser. International Series in Operations Research & Management Science. New York, NY, USA: Springer, 1998, vol. 12.
- [37] D. W. Matolak and R. Sun, “Air-ground channel characterization for unmanned aircraft systems-part III: The suburban and near-urban environments,” *IEEE Trans. Veh. Technol.*, vol. 66, no. 8, pp. 6607–6618, 2017.
- [38] S. Boyd and L. Vandenberghe, *Convex Optimization*. Cambridge University Press, 2004.
- [39] M. Grant and S. Boyd, “CVX: Matlab software for disciplined convex programming, version 2.1,” <https://cvxr.com/cvx>, Mar. 2014.
- [40] R. K. Ahuja, T. L. Magnanti, and J. B. Orlin, *Network Flows: Theory, Algorithms, and Applications*. Prentice Hall, 1993.
- [41] K. Gatsis, A. Ribeiro, and G. J. Pappas, “Optimal power management in wireless control systems,” *IEEE Trans. Autom. Control*, vol. 59, no. 6, pp. 1495–1510, 2014.
- [42] S. M. Ross, *Introduction to probability models*. Academic press, 2014.
- [43] J.-W. Lee and J.-A. Kwon, “Utility-based power allocation for multiclass wireless systems,” *IEEE Trans. Veh. Technol.*, vol. 58, no. 7, pp. 3813–3819, 2009.
- [44] S. Vaidanis, P. A. Stavrou, and M. Kountouris, “Goal-oriented semantic resource allocation with cumulative prospect theoretic agents,” in *Proc. IEEE Int. Conf. Commun.*, 2025, pp. 4154–4159.
- [45] “Evolved universal terrestrial radio access (E-UTRA); further advancements for E-UTRA physical layer aspects,” 3GPP, Tech. Rep. TR 36.814 (Release 9), Mar. 2017.
- [46] M. Mozaffari, W. Saad, M. Bennis, and M. Debbah, “Mobile unmanned aerial vehicles (UAVs) for energy-efficient internet of things communications,” *IEEE Trans. Wireless Commun.*, vol. 16, no. 11, pp. 7574–7589, 2017.
- [47] M. Zarepisheh and P. M. Pardalos, “An equivalent transformation of multi-objective optimization problems,” *Annals of Operations Research*, vol. 249, no. 1, pp. 5–15, 2017.
- [48] F. Neussel and O. Stein, “On image space transformations in multiobjective optimization,” 2025. [Online]. Available: <https://optimization-online.org/?p=30125>
- [49] B. Schröder, *Ordered sets: An introduction*. Springer, 2016, vol. 328.
- [50] A. J. Hoffman and J. B. Kruskal, “Integral boundary points of convex polyhedra,” in *50 Years of Integer Programming 1958–2008: From the Early Years to the State-of-the-Art*. Springer, 2009, pp. 49–76.

Appendix A Proof of Theorem 1

The total energy consumption in the objective function of $\mathcal{P}3$ is additive over time. By partitioning the time horizon into $|\mathcal{I}|$ disjoint intervals defined by \mathbf{t} , the objective function can be expanded as

$$E = \sum_{i \in \mathcal{I}} \sum_{n \in \mathcal{N}, k \in \mathcal{K}, t \in \mathcal{T}_i} a_n[k, t] p_n[k, t].$$

For any feasible \mathbf{t} , the time intervals $\mathcal{T}_i \triangleq [t_i, t_{i+1}) \cap \mathbb{Z}_+$ are deterministic and disjoint over i . Consequently, the local policy variables $\mathcal{A}_i = \{a_n[k, t]\}_{n \in \mathcal{N}, k \in \mathcal{K}, t \in \mathcal{T}_i}$ and $\mathcal{P}_i = \{p_n[k, t]\}_{n \in \mathcal{N}, k \in \mathcal{K}, t \in \mathcal{T}_i}$ are mutually strictly coupled only within their respective intervals. Specifically, the constraints in (23) and the policy feasibility $\mathcal{A} \in \mathcal{S}_{\mathbf{A}}^{|\mathcal{I}|}$ and $\mathcal{P} \in \mathcal{S}_{\mathbf{P}}^{|\mathcal{I}|}$ apply independently to each interval i .

Similarly, the constraint $\theta(\boldsymbol{\pi}) \leq \varepsilon_\theta$, as defined in (12), is equivalent to

$$\sum_{k \in \mathcal{K}} a_n[k, t] \leq \varepsilon_\theta, \forall n \in \mathcal{N}, t \in \mathcal{T}_i,$$

for all $i \in \mathcal{I}$. As a result, the constraint $\theta(\boldsymbol{\pi}) \leq \varepsilon_\theta$ can be decoupled into I independent constraints.

Due to this block-separable structure of both the objective function and the constraints, the minimization over the global power and RB allocation policy, i.e., \mathcal{A} and \mathcal{P} , decomposes into a summation of independent subproblems

$$\begin{aligned} & \underset{\mathcal{A}_i, \mathcal{P}_i}{\text{minimize}} && \sum_{n \in \mathcal{N}, k \in \mathcal{K}, t \in \mathcal{T}_i} a_n[k, t] p_n[k, t] \\ & \text{subject to} && \mathbb{E}\{v(t_i, t_{i+1})\} \geq \bar{v}, \\ & && \sum_{k \in \mathcal{K}} a_n[k, t] \leq \varepsilon_\theta, \forall n \in \mathcal{N}, t \in \mathcal{T}_i, \\ & && \mathcal{A}_i \in \mathcal{S}_{\mathbf{A}}^{|\mathcal{T}_i|}, \mathcal{P}_i \in \mathcal{S}_{\mathbf{P}}^{|\mathcal{T}_i|}. \end{aligned}$$

Let $E^*(t_i, t_{i+1})$ denote the optimal value of the inner minimization term for the i th interval. Substituting this back into the global problem $\mathcal{P}3$ and optimizing over the remaining variable \mathbf{t} , we obtain the equivalent master problem

$$\min_{\mathbf{t}} \sum_{i \in \mathcal{I}} E^*(t_i, t_{i+1}) \quad \text{s.t. } \mathbf{t} \in \Upsilon.$$

Appendix B

Proof of Theorem 2

To establish the order-preserving equivalence between $\mathcal{P}1$ and $\mathcal{P}1^v$, we formalize the preservation of dominance relations under the monotone cost mapping, similar to [47], [48]. According to the definition of Pareto optimality in Definition 1, a policy $\boldsymbol{\pi} \in \Pi$ is efficient for $\mathcal{P}1$ if there exists no $\boldsymbol{\pi}' \in \Pi$ such that $\mathbf{f}(\boldsymbol{\pi}') \preceq \mathbf{f}(\boldsymbol{\pi})$, where $\mathbf{f}(\boldsymbol{\pi}) \triangleq (\theta(\boldsymbol{\pi}), E(\boldsymbol{\pi}))^T$. Similarly, $\boldsymbol{\pi} \in \Pi$ is efficient for $\mathcal{P}1-1$ if there exists no $\boldsymbol{\pi}' \in \Pi$ such that $\mathbf{g}(\mathbf{f}(\boldsymbol{\pi}')) \preceq \mathbf{g}(\mathbf{f}(\boldsymbol{\pi}))$.

Since each cost function $g_j(\cdot)$ is strictly increasing, the mapping $g(\cdot)$ constitutes an order isomorphism between the original objective space $\mathbf{f}(\boldsymbol{\pi})$ and the cost space $\mathbf{g}(\mathbf{f}(\boldsymbol{\pi}))$ [49, Proposition 1.3.5]. Consequently, the dominance relations are preserved such that

$$\mathbf{f}(\boldsymbol{\pi}') \preceq \mathbf{f}(\boldsymbol{\pi}) \iff \mathbf{g}(\mathbf{f}(\boldsymbol{\pi}')) \preceq \mathbf{g}(\mathbf{f}(\boldsymbol{\pi})).$$

Now, let Π_f^* and Π_g^* denote Pareto-optimal sets for $\mathcal{P}1$ and $\mathcal{P}1-1$, respectively. If $\boldsymbol{\pi} \in \Pi_f^*$ then for all $\boldsymbol{\pi}' \in \Pi$, $\mathbf{f}(\boldsymbol{\pi}') \not\preceq \mathbf{f}(\boldsymbol{\pi})$. By the isomorphism above, this holds if and only if $\mathbf{g}(\mathbf{f}(\boldsymbol{\pi}')) \not\preceq \mathbf{g}(\mathbf{f}(\boldsymbol{\pi}))$ for all $\boldsymbol{\pi}' \in \Pi$, which implies $\boldsymbol{\pi} \in \Pi_g^*$. Conversely, if $\boldsymbol{\pi} \in \Pi_g^*$, the same logic implies $\boldsymbol{\pi} \in \Pi_f^*$. Thus, $\Pi_f^* = \Pi_g^*$, proving that the set of efficient policies for both problems coincides exactly.

Finally, the Pareto frontier in the cost space is obtained by

$$\begin{aligned} \mathcal{C}_g &= \{\mathbf{g}(\mathbf{f}(\boldsymbol{\pi})) \mid \boldsymbol{\pi} \in \Pi_g^*\} = \{\mathbf{g}(\mathbf{f}(\boldsymbol{\pi})) \mid \boldsymbol{\pi} \in \Pi_f^*\} \\ &= \{(g_1(\theta), g_2(E)) : (\theta, E) \in \mathcal{C}\}. \end{aligned}$$

Appendix C
Proof of Proposition 1

We will prove that any point in \mathcal{C} is Pareto-optimal for Problem $\mathcal{P}1$ and all Pareto-optimal points of $\mathcal{P}1$ lie on \mathcal{C} . To establish this result, we first prove two key lemmas concerning the monotonicity of the $E^*(\varepsilon_\theta)$.

A. Monotonicity of $E^*(\varepsilon_\theta)$

Lemma 2: For any $\varepsilon_{\theta,1} < \varepsilon_{\theta,2}$, $E^*(\varepsilon_{\theta,1}) \geq E^*(\varepsilon_{\theta,2})$.

Proof: Given any $\varepsilon_{\theta,1} < \varepsilon_{\theta,2}$, we will first prove $\mathcal{F}(\varepsilon_{\theta,1}) \subseteq \mathcal{F}(\varepsilon_{\theta,2})$, where $\mathcal{F}(\varepsilon_\theta)$ is the feasible set of Problem $\mathcal{P}2$ under load cap ε_θ , i.e.,

$$\mathcal{F}(\varepsilon_\theta) = \{\boldsymbol{\pi} \in \Pi : \tau[t] \leq \bar{\tau}, \forall t \text{ and } \theta(\boldsymbol{\pi}) \leq \varepsilon_\theta\}. \quad (40)$$

If $\mathcal{F}(\varepsilon_{\theta,1}) = \emptyset$, we have $\mathcal{F}(\varepsilon_{\theta,1}) \subseteq \mathcal{F}(\varepsilon_{\theta,2})$. Otherwise, $\mathcal{F}(\varepsilon_{\theta,1}) \neq \emptyset$, for any $\boldsymbol{\pi} \in \mathcal{F}(\varepsilon_{\theta,1})$, the load cap constraint ensures

$$\theta(\boldsymbol{\pi}) = \sum_{k \in \mathcal{K}} a_n[k, t] \leq \varepsilon_{\theta,1} < \varepsilon_{\theta,2}, \forall n, t.$$

Moreover, all other constraints are independent of ε_θ , the policy $\boldsymbol{\pi}$ also satisfies (15) and (16). Therefore, $\boldsymbol{\pi} \in \mathcal{F}(\varepsilon_{\theta,2})$ according to its definition in (40), which establishes $\mathcal{F}(\varepsilon_{\theta,1}) \subseteq \mathcal{F}(\varepsilon_{\theta,2})$.

Minimizing the same objective E in $\mathcal{P}2$, over a larger feasible set, yields a lower optimum. Therefore,

$$E^*(\varepsilon_{\theta,1}) \geq E^*(\varepsilon_{\theta,2}), \forall \varepsilon_{\theta,1} < \varepsilon_{\theta,2},$$

showing that $E^*(\varepsilon_\theta)$ is non-increasing over ε_θ . \blacksquare

Lemma 3: For any $\varepsilon_{\theta,1} < \varepsilon_{\theta,2}$ with $\varepsilon_{\theta,1}, \varepsilon_{\theta,2} \in [\underline{\theta}, \bar{\theta}] \cap \mathbb{Z}_+$, $E^*(\varepsilon_{\theta,1}) > E^*(\varepsilon_{\theta,2})$.

Proof: We prove this by contradiction. Suppose that there exist $\underline{\theta} \leq \varepsilon_{\theta,1} < \varepsilon_{\theta,2} \leq \bar{\theta}$, such that $E^*(\varepsilon_{\theta,1}) = E^*(\varepsilon_{\theta,2})$. Let $\boldsymbol{\pi}^* \in \mathcal{F}(\varepsilon_{\theta,1})$ be any optimal policy for Problem $\mathcal{P}2$ given the constraint $\varepsilon_{\theta,1}$. By definition, $\theta(\boldsymbol{\pi}^*) \leq \varepsilon_{\theta,1}$ and $E(\boldsymbol{\pi}^*) = E^*(\varepsilon_{\theta,1})$. Since $\varepsilon_{\theta,1} < \varepsilon_{\theta,2}$, it follows $\mathcal{F}(\varepsilon_{\theta,1}) \subseteq \mathcal{F}(\varepsilon_{\theta,2})$ according to Lemma 2. Consequently, $\boldsymbol{\pi}^*$ is feasible for the problem with relaxed constraint $\varepsilon_{\theta,2}$.

Given the assumption $E^*(\varepsilon_{\theta,1}) = E^*(\varepsilon_{\theta,2})$, the policy $\boldsymbol{\pi}^*$ is also optimal for Problem $\mathcal{P}2$ under constraint $\varepsilon_{\theta,2}$, satisfying the resource inequality strictly

$$\theta(\boldsymbol{\pi}^*) \leq \varepsilon_{\theta,1} < \varepsilon_{\theta,2}.$$

The strict slackness of the constraint implies that the constraint $\theta(\boldsymbol{\pi}^*) < \varepsilon_{\theta,2}$ is inactive. From the principles of multiobjective optimization [36, Theorem 3.2.2], if relaxing a constraint yields no improvement in the objective function, the objective must have reached its local unconstrained minimum with respect to that resource. Thus, the system is saturated at $\varepsilon_{\theta,1}$, implying

$$E^*(\varepsilon_{\theta,1}) = E^* \Rightarrow \bar{\theta} \leq \varepsilon_{\theta,1},$$

which contradicts the initial assumption that $\varepsilon_{\theta,1} < \varepsilon_{\theta,2} \leq \bar{\theta}$ (specifically $\varepsilon_{\theta,1} < \bar{\theta}$).

Therefore, the assumption is false, and we conclude that $E^*(\varepsilon_{\theta,1}) > E^*(\varepsilon_{\theta,2})$ for any $\varepsilon_{\theta,1} < \varepsilon_{\theta,2}$ with $\varepsilon_{\theta,1}, \varepsilon_{\theta,2} \in [\underline{\theta}, \bar{\theta}] \cap \mathbb{Z}_+$. \blacksquare

B. Points on \mathcal{C} are Pareto-optimal

We prove this by contradiction. Suppose that a point $(\varepsilon_\theta, E^*(\varepsilon_\theta))$ with $\varepsilon_\theta \in [\underline{\theta}, \bar{\theta}] \cap \mathbb{Z}_+$ is not Pareto-optimal. This implies the existence of a feasible pair (θ', E') that dominates $(\varepsilon_\theta, E^*(\varepsilon_\theta))$, meaning

$$\theta' \leq \varepsilon_\theta, E' \leq E^*(\varepsilon_\theta), \text{ and } (\varepsilon_\theta, E^*(\varepsilon_\theta)) \neq (\theta', E').$$

First, by the definition of the optimal value function $E^*(\cdot)$, any feasible pair must satisfy $E' \geq E^*(\theta')$. Combining this with the dominance condition yields

$$E^*(\theta') \leq E' \leq E^*(\varepsilon_\theta). \quad (41)$$

We consider two cases for θ' . Case $\theta' < \varepsilon_\theta$: Since $\varepsilon_\theta \leq \bar{\theta}$, strict monotonicity from Lemma 3 implies $E^*(\theta') > E^*(\varepsilon_\theta)$. This directly contradicts inequality (41). Case $\theta' = \varepsilon_\theta$: Inequality (41) implies $E^*(\varepsilon_\theta) \leq E' \leq E^*(\varepsilon_\theta)$, forcing $E' = E^*(\varepsilon_\theta)$. Thus, $(\varepsilon_\theta, E^*(\varepsilon_\theta)) = (\theta', E')$, which contradicts the requirement that a dominating point must be distinct from the original point.

Thus, we conclude that since no such dominating pair exists, every point on \mathcal{C} is Pareto-optimal.

C. Every Pareto-Optimal Feasible Pair Lies on \mathcal{C} .

Let (θ', E') be any Pareto-optimal point. We will prove $(\theta', E') \in \mathcal{C}$, that is $E' = E^*(\theta')$ and $\theta' \leq \bar{\theta}$.

Feasibility implies $E' \geq E^*(\theta')$. If $E' > E^*(\theta')$, the point $(\theta', E^*(\theta'))$ is feasible and strictly dominates (θ', E') . Thus, Pareto optimality necessitates $E' = E^*(\theta')$.

Suppose $\theta' > \bar{\theta}$. By the definition of the saturation point $\bar{\theta}$ in (17), we have $E^*(\theta') = E^*(\bar{\theta})$. It implies consuming strictly less resource for the same energy performance. Thus, Pareto optimality necessitates $\theta' \leq \bar{\theta}$.

Combining these results, any Pareto-optimal point must satisfy $E' = E^*(\theta')$ and $\theta' \leq \bar{\theta}$, which is exactly the definition of \mathcal{C} .

Appendix D
Proof of Lemma 1

Define a new random variable $Y = \ln(\gamma_n[k, t])$, such that $\gamma_n[k, t] = e^Y$. Substituting this into the capacity equation

$$\mathbb{E}\{c_n[k, t]\} = \mathbb{E}_Y \{\log_2(1 + e^Y)\}.$$

Consider the auxiliary function $f(y) = \log_2(1 + e^y)$. We examine its convexity by computing the second derivative with respect to y

$$f'(y) = \frac{1}{\ln 2} \frac{e^y}{1 + e^y}, f''(y) = \frac{1}{\ln 2} \frac{e^y}{(1 + e^y)^2}.$$

Since $e^y > 0$ for all real y , the second derivative $f''(y)$ is strictly positive. Thus, $f(y)$ is a strictly convex function. Applying Jensen's inequality to the capacity equation, we have

$$\mathbb{E}_Y \{\log_2(1 + e^Y)\} \geq \log_2(1 + e^{\mathbb{E}\{Y\}}).$$

According to the definition of $\gamma_n[k, t]$ in (6) and $h_n[k, t]$ in (1), $\gamma_n[k, t]$ is a Gamma-distributed variable

$$\gamma_n[k, t] \sim \text{Gamma}\left(\kappa_n[k, t], \frac{p_n[k, t] g_n[k, t]}{\delta^2 \kappa_n[k, t]}\right).$$

Then, the expected value of its natural logarithm is known in closed form

$$\begin{aligned} & \mathbb{E} \{ \ln (\gamma_n [k, t]) \} \\ &= \psi (\kappa_n [k, t]) + \ln \left(\underbrace{\frac{p_n [k, t] g_n [k, t]}{\delta^2}}_{\bar{\gamma}_n [k, t]} \frac{1}{\kappa_n [k, t]} \right). \end{aligned}$$

where $\psi (\cdot)$ is the Digamma function. Substituting this back into the exponential term

$$e^{\mathbb{E}\{Y\}} = e^{\psi(\kappa_n[k,t]) + \ln(\frac{\bar{\gamma}_n[k,t]}{\kappa_n[k,t]})} = \frac{e^{\psi(\kappa_n[k,t])}}{\kappa_n[k,t]} \bar{\gamma}_n[k,t].$$

Define the scaling coefficient $\beta_n [k, t] = e^{\psi(\kappa_n[k,t])} / \kappa_n [k, t]$. Substituting back into the Jensen bound, we have

$$\mathbb{E} \{ c_n [k, t] \} \geq \log_2 (1 + \beta_n [k, t] \bar{\gamma}_n [k, t]). \quad (42)$$

Next, we analyze the tightness of the lower bound. As $\kappa_n [k, t] \rightarrow \infty$, the asymptotic expansion of the digamma function gives

$$\psi (\kappa_n [k, t]) = \ln (\kappa_n [k, t]) - \frac{1}{2 \kappa_n [k, t]} + O \left(\frac{1}{\kappa_n^2 [k, t]} \right),$$

which implies $\beta_n [k, t] \rightarrow 1$. Then, (42) becomes

$$\mathbb{E} \{ c_n [k, t] \} \geq \log_2 (1 + \bar{\gamma}_n [k, t]). \quad (43)$$

Moreover, since $\log_2 (1 + x)$ is concave, Jensen's inequality yields

$$\mathbb{E} \{ c_n [k, t] \} \leq \log_2 (1 + \mathbb{E} \{ \bar{\gamma}_n [k, t] \}) = \log_2 (1 + \bar{\gamma}_n [k, t]). \quad (44)$$

Combining (43) and (44), we have

$$\lim_{\kappa_n [k, t] \rightarrow \infty} (\mathbb{E} \{ c_n [k, t] \} - \bar{c}_n [k, t]) = 0.$$

As $\bar{\gamma}_n [k, t] \rightarrow \infty$, we have

$$\mathbb{E} \{ \log_2 (1 + \gamma_n [k, t]) \} = \mathbb{E} \{ \log_2 (\bar{\gamma}_n [k, t]) \} + o(1).$$

Then, according to the expected value of its natural logarithm, we have

$$\mathbb{E} \{ \log_2 (\gamma_n [k, t]) \} = \frac{1}{\ln 2} \left(\psi (\kappa_n [k, t]) + \ln \frac{\bar{\gamma}_n [k, t]}{\kappa_n [k, t]} \right).$$

Using $\beta_n [k, t] = e^{\psi(\kappa_n[k,t])} / \kappa_n [k, t]$, this becomes

$$\mathbb{E} \{ \log_2 (\gamma_n [k, t]) \} = \log_2 (\beta_n [k, t] \bar{\gamma}_n [k, t]).$$

On the other hand,

$$\log_2 (1 + \beta_n [k, t] \bar{\gamma}_n [k, t]) = \log_2 (\beta_n [k, t] \bar{\gamma}_n [k, t]) + o(1).$$

Therefore,

$$\lim_{\bar{\gamma}_n [k, t] \rightarrow \infty} (\mathbb{E} \{ c_n [k, t] \} - \bar{c}_n [k, t]) = 0.$$

Appendix E

Proof of Proposition 2, 3 and 4

We prove Proposition 2 via the KKT conditions of $\mathcal{P}4$, constructing an explicit primal-dual policy, and verifying that it satisfies all KKT conditions. Since $\mathcal{P}4$ is convex and satisfies Slater's condition, the KKT conditions are necessary and sufficient for optimality [38, Section 5.5.3].

A. Necessary and Sufficient Optimality Conditions

Introduce Lagrange multiplier λ , $\{\mu_1[t]\}_{t \in \mathcal{T}_i}$, $\{\mu_2[n, t]\}_{n \in \mathcal{N}, t \in \mathcal{T}_i}$, $\{\mu_3[k, t]\}_{k \in \mathcal{K}, t \in \mathcal{T}_i}$, and $\{\mu_4[n, k, t], \mu_5[n, k, t], \mu_6[n, k, t]\}_{n \in \mathcal{N}, k \in \mathcal{K}, t \in \mathcal{T}_i}$, associated with the constraints in $\mathcal{P}4$. The Lagrangian is

$$\begin{aligned} \mathcal{L} = & \sum_{n \in \mathcal{N}, k \in \mathcal{K}, t \in \mathcal{T}_i} \iota_n [k, t] a_n [k, t] \left(2^{\frac{\phi_n [k, t]}{a_n [k, t]}} - 1 \right) \\ & + \lambda \left(\bar{v} - \sum_{n \in \mathcal{N}, k \in \mathcal{K}, t \in \mathcal{T}_i} \phi_n [k, t] \right) \\ & + \sum_{t \in \mathcal{T}_i} \mu_1 [t] \left(\sum_{n \in \mathcal{N}, k \in \mathcal{K}} \iota_n [k, t] a_n [k, t] \left(2^{\frac{\phi_n [k, t]}{a_n [k, t]}} - 1 \right) - \bar{p} \right) \\ & + \sum_{n \in \mathcal{N}, t \in \mathcal{T}_i} \mu_2 [n, t] \left(\sum_{k \in \mathcal{K}} a_n [k, t] - \varepsilon_\theta \right) \\ & + \sum_{k \in \mathcal{K}, t \in \mathcal{T}_i} \mu_3 [k, t] \left(\sum_{n \in \mathcal{N}} a_n [k, t] - 1 \right) \\ & + \sum_{n \in \mathcal{N}, k \in \mathcal{K}, t \in \mathcal{T}_i} \mu_4 [n, k, t] (-a_n [k, t]) \\ & + \sum_{n \in \mathcal{N}, k \in \mathcal{K}, t \in \mathcal{T}_i} \mu_5 [n, k, t] (a_n [k, t] - 1) \\ & + \sum_{n \in \mathcal{N}, k \in \mathcal{K}, t \in \mathcal{T}_i} \mu_6 [n, k, t] (-\phi_n [k, t]). \end{aligned}$$

The KKT conditions for $\mathcal{P}4$ consist of 1) Primal and dual feasibility: Constraints of $\mathcal{P}4$ and non-negativity of multipliers; 2) Complementary slackness

$$\lambda \left(\bar{v} - \sum_{n \in \mathcal{N}, k \in \mathcal{K}, t \in \mathcal{T}_i} \phi_n [k, t] \right) = 0, \quad (45)$$

$$\mu_1 [t] \left(\sum_{n \in \mathcal{N}, k \in \mathcal{K}} \iota_n [k, t] a_n [k, t] \left(2^{\frac{\phi_n [k, t]}{a_n [k, t]}} - 1 \right) - \bar{p} \right) = 0, \quad \forall t \in \mathcal{T}_i, \quad (46)$$

$$\mu_2 [n, t] \left(\sum_{k \in \mathcal{K}} a_n [k, t] - \varepsilon_\theta \right) = 0, \quad \forall n \in \mathcal{N}, t \in \mathcal{T}_i, \quad (47)$$

$$\mu_3 [k, t] \left(\sum_{n \in \mathcal{N}} a_n [k, t] - 1 \right) = 0, \quad \forall k \in \mathcal{K}, t \in \mathcal{T}_i, \quad (48)$$

$$\mu_4 [n, k, t] (-a_n [k, t]) = 0, \quad \forall n \in \mathcal{N}, k \in \mathcal{K}, t \in \mathcal{T}_i, \quad (49)$$

$$\mu_5 [n, k, t] (a_n [k, t] - 1) = 0, \quad \forall n \in \mathcal{N}, k \in \mathcal{K}, t \in \mathcal{T}_i, \quad (50)$$

$$\mu_6 [n, k, t] (-\phi_n [k, t]) = 0, \quad \forall n \in \mathcal{N}, k \in \mathcal{K}, t \in \mathcal{T}_i. \quad (51)$$

3) Stationarity

$$\frac{\partial \mathcal{L}}{\partial \phi_n [k, t]} = 0, \quad \forall n \in \mathcal{N}, k \in \mathcal{K}, t \in \mathcal{T}_i, \quad (52)$$

$$\frac{\partial \mathcal{L}}{\partial a_n [k, t]} = 0, \quad \forall n \in \mathcal{N}, k \in \mathcal{K}, t \in \mathcal{T}_i. \quad (53)$$

In the sequel, we derive the optimal policy from these conditions.

B. Optimal Spectral Efficiency (Water-Filling)

Taking the partial derivative with respect to $\phi_n[k, t]$ in (52), and substituting $\bar{c}_n[k, t] = \phi_n[k, t]/a_n[k, t]$, we have

$$(1 + \mu_1[t]) \iota_n[k, t] \ln 2 \cdot 2^{\bar{c}_n[k, t]} - \lambda - \mu_6[n, k, t] = 0. \quad (54)$$

If $\bar{c}_n[k, t] > 0$, then $a_n[k, t] > 0$ according to the definition of $p_n[k, t]$ in (28). We have $\mu_6[n, k, t] = 0$ according to (51), then (54) becomes

$$(1 + \mu_1[t]) \iota_n[k, t] \ln 2 \cdot 2^{\bar{c}_n[k, t]} - \lambda = 0.$$

Solving for $\bar{c}_n[k, t]$ and ensuring non-negativity, we have

$$\bar{c}_n^*[k, t] = \left[\log_2 \left(\underbrace{\frac{\lambda}{\ln 2 (1 + \mu_1[t])}}_{\triangleq \lambda_t} \frac{1}{\iota_n[k, t]} \right) \right]^+. \quad (55)$$

Thus, the optimal power allocation is

$$p_n^*[k, t] = [\lambda_t - \iota_n[k, t]]^+. \quad (56)$$

C. Optimal RB Allocation

Similarly, taking the partial derivative with respect to $a_n[k, t]$ in (53), and substituting $\bar{c}_n[k, t] = \phi_n[k, t]/a_n[k, t]$, we have

$$\underbrace{(1 + \mu_1[t]) \iota_n[k, t] \left(2^{\bar{c}_n[k, t]} (1 - \ln 2 \bar{c}_n[k, t]) - 1 \right)}_{H_n[k, t]} + \mu_2[n, t] + \mu_3[k, t] - \mu_4[n, k, t] + \mu_5[n, k, t] = 0. \quad (57)$$

The stationarity condition (57) with corresponding complementary slackness conditions (47)–(50) can be equivalently viewed from a Lagrangian function $\mathcal{L}_2 = \sum_{t \in \mathcal{T}_i} \mathcal{L}_3[t]$, where $\mathcal{L}_3[t]$ is defined as

$$\begin{aligned} \mathcal{L}_3[t] &= \sum_{n \in \mathcal{N}, k \in \mathcal{K}} H_n[k, t] a_n[k, t] \\ &+ \sum_{n \in \mathcal{N}} \mu_2[n, t] \left(\sum_{k \in \mathcal{K}} a_n[k, t] - \varepsilon_\theta \right) \\ &+ \sum_{k \in \mathcal{K}} \mu_3[k, t] \left(\sum_{n \in \mathcal{N}} a_n[k, t] - 1 \right) \\ &+ \sum_{n \in \mathcal{N}, k \in \mathcal{K}} \mu_4[n, k, t] (-a_n[k, t]) \\ &+ \sum_{n \in \mathcal{N}, k \in \mathcal{K}} \mu_5[n, k, t] (a_n[k, t] - 1). \end{aligned}$$

This Lagrangian function $\mathcal{L}_3[t]$ corresponds to the following RB allocation problem

$$\underset{\{a_n[k, t]\}_{n \in \mathcal{N}, k \in \mathcal{K}}}{\text{minimize}} \sum_{n \in \mathcal{N}, k \in \mathcal{K}} H_n[k, t] a_n[k, t], \quad (58)$$

$$\text{subject to} \sum_{k \in \mathcal{K}} a_n[k, t] \leq \varepsilon_\theta, \forall n \in \mathcal{N}, \quad (59)$$

$$\sum_{n \in \mathcal{N}} a_n[k, t] \leq 1, \forall k \in \mathcal{K}, \quad (60)$$

$$a_n[k, t] \in [0, 1], \forall n \in \mathcal{N}, k \in \mathcal{K}. \quad (61)$$

By substituting the optimal $\bar{c}_n^*[k, t]$ in (55) into $H_n[k, t]$, we can express $H_n[k, t]$ as

$$\begin{aligned} H_n[k, t] &= (1 + \mu_1[t]) \iota_n[k, t] \left(2^{\bar{c}_n^*[k, t]} (1 - \ln 2 \bar{c}_n^*[k, t]) - 1 \right) \\ &= (1 + \mu_1[t]) (\lambda_t - \iota_n[k, t] - \ln 2 \lambda_t \bar{c}_n^*[k, t]) \\ &= \underbrace{(1 + \mu_1[t])}_{\geq 1} (p_n^*[k, t] - \ln 2 \lambda_t \bar{c}_n^*[k, t]). \end{aligned}$$

Denote $w_n[k, t] = p_n^*[k, t] - \ln 2 \lambda_t \bar{c}_n^*[k, t]$, therefore, the optimal RB allocation $\mathbf{A}^*[t; \lambda_t]$ is the solution to

$$\underset{\mathbf{A}[t] \in \mathcal{A}(t)}{\text{min}} \sum_{n \in \mathcal{N}, k \in \mathcal{K}} w_n[k, t] a_n[k, t] \text{ s.t. (59)–(61)}. \quad (62)$$

D. Capped Water Level

Denote $\tilde{\lambda}_t$ as the solution to $p^*[t; \Lambda] = \bar{p}$. Then, complementary slackness (46) implies two regimes

- Inactive constraint ($p^*[t; \tilde{\lambda}_t] < \bar{p}$): It means $\mu_1[t] = 0$, yielding $\lambda_t = \lambda / \ln 2$;
- Active constraint ($p^*[t; \tilde{\lambda}_t] = \bar{p}$): It implies $\lambda_t = \tilde{\lambda}_t$.

Equivalently, the optimal effective water level is the capped value

$$\lambda_t = \min \left\{ \frac{\lambda}{\ln 2}, \tilde{\lambda}_t \right\}. \quad (63)$$

E. Optimal Lagrangian Parameter

Since $\bar{c}_n^*[k, t; \lambda_t] a_n^*[k, t; \lambda_t] > 0$ if and only if $\lambda_t > 0$ (i.e., $\lambda > 0$), any strictly positive rate requirement $\bar{v} > 0$ implies $\lambda > 0$. Thus, the rate constraint is active according to (45), and the optimal λ is the unique solution to the following equation

$$\sum_{n \in \mathcal{N}, k \in \mathcal{K}, t \in \mathcal{T}_i} \bar{c}_n^*[k, t; \lambda_t] a_n^*[k, t; \lambda_t] = \bar{v}. \quad (64)$$

F. Optimal Binary RB Policy

We will prove that there exists an optimal binary RB allocation policy for any λ_t , i.e., $a_n^*[k, t] \in \{0, 1\}$ for all $n \in \mathcal{N}$ and $k \in \mathcal{K}$.

Stack the variables $\mathbf{A}[t]$ for any t into a vector

$$\mathbf{x}_t \triangleq [a_1[1, t], \dots, a_1[K, t], a_2[1, t], \dots, a_2[K, t], \dots, a_N[1, t], \dots, a_N[K, t]]^T.$$

With this definition, problem (62) can be written in standard linear programming form as

$$\underset{\mathbf{x}_t}{\text{min}} \mathbf{w}_t^T \mathbf{x}_t, \text{ s.t. } \mathbf{M} \mathbf{x}_t \leq \mathbf{b}, \mathbf{x}_t \geq 0,$$

where vector \mathbf{w}_t collects the coefficients of $w_n[k, t]$, and the constraint matrix \mathbf{M} and right-hand side vector \mathbf{b} are given by

$$\mathbf{M} = \begin{bmatrix} \mathbf{I}_N \otimes \mathbf{1}_K^T \\ \mathbf{1}_N^T \otimes \mathbf{I}_K \end{bmatrix}, \mathbf{b} = \begin{bmatrix} \varepsilon_\theta \mathbf{1}_N \\ \mathbf{1}_K \end{bmatrix}.$$

Note that $\sum_{n \in \mathcal{N}} a_n[k, t] \leq 1$ and $a_n[k, t] \geq 0$ imply $a_n[k, t] \leq 1$. Thus, the explicit upper bound constraint is redundant.

Each column of \mathbf{M} contains exactly two nonzero entries, both equal to 1, and the rows of \mathbf{M} can be partitioned into two disjoint sets corresponding to user constraints and resource-block constraints, with each column having at most one nonzero entry in each set. Hence, \mathbf{M} is a totally unimodular matrix [50]. Moreover, since $\varepsilon_\theta \in \mathbb{Z}_+$, the vector \mathbf{b} is integral. By the Hoffman-Kruskal theorem [50], problem (62) has integer optima, i.e., $a_n^*[k, t] \in \{0, 1\}$ for all $n \in \mathcal{N}$ and $k \in \mathcal{K}$.

G. Optimality, Continuity and Monotonicity

Define the per-slot sum rate and the consumed power at slot t as

$$\Phi^*[t; \Lambda] \triangleq \sum_{n \in \mathcal{N}, k \in \mathcal{K}} \bar{c}_n^*[k, t; \Lambda] a_n^*[k, t; \Lambda], \quad (65)$$

$$P^*[t; \Lambda] \triangleq \sum_{n \in \mathcal{N}, k \in \mathcal{K}} p_n^*[k, t; \Lambda] a_n^*[k, t; \Lambda], \quad (66)$$

where $\Lambda \geq 0$. Since the optimal control variables $\{\bar{c}_n^*[k, t; \Lambda], p_n^*[k, t; \Lambda], a_n^*[k, t; \Lambda]\}$ derived in Sections E-B and E-C are determined by Λ , both $\phi^*[t; \Lambda]$ and $p^*[t; \Lambda]$ can be viewed as functions of Λ .

We define the set of switching points where the binary allocation changes as

$$\mathcal{S}_s = \left\{ \Lambda_0 \geq 0; \mathbf{A}^*[t; \Lambda_0] \neq \lim_{\Lambda \rightarrow \Lambda_0} \mathbf{A}^*[t; \Lambda] \right\},$$

where $\mathbf{A}^*[t; \Lambda_0]$ is the integer solution to (62). The remaining non-switching domain is defined as

$$\mathcal{S}_{\text{ns}} = \bigcup_{i \in \{0, \dots, |\mathcal{S}_s|\}} s_i, \quad s_i = (\mathcal{S}_s[i], \mathcal{S}_s[i+1]),$$

where $\mathcal{S}_s[i]$ denotes the i th smallest point in $\mathcal{S}_s \cup \{0, \infty\}$. It is clear that the closure of these sets satisfies $\mathcal{S}_s \cup \mathcal{S}_{\text{ns}} = \mathbb{R}_{0+}$.

For the first segment s_0 (where $0 \leq \Lambda < \iota_n[k, t]$), all RBs are inactive, yielding $\phi^*[t; \Lambda] = 0$ and $p^*[t; \Lambda] = 0$. For each subsequent segment s_i with $i > 1$, the RB allocation $\mathbf{A}^*[t; \Lambda]$ remains constant. Consequently, both $\phi^*[t; \Lambda]$ and $p^*[t; \Lambda]$ are finite linear combinations of $\{\bar{c}_n^*[k, t; \Lambda]\}$ and $\{p_n^*[k, t; \Lambda]\}$ which are continuously increasing in Λ . Thus, $\phi^*[t; \Lambda]$ and $p^*[t; \Lambda]$ are continuous and strictly increasing over any interval $\Lambda \in s_i$.

Next, we analyze the behavior at the switching points. Since the problem (62) has a continuous objective and a compact feasible set, its optimal objective value is continuous in Λ . Evaluating the optimality condition at a switching point Λ (where $\Lambda^- = \Lambda = \Lambda^+$), we have

$$p^*[t; \Lambda^-] - \ln 2\Lambda \phi^*[t; \Lambda^-] = p^*[t; \Lambda^+] - \ln 2\Lambda \phi^*[t; \Lambda^+]. \quad (67)$$

Since $\Lambda > 0$, the change in power and sum rate must share the same sign.

The optimality of the policy at Λ^- implies it minimizes the Lagrangian at that specific water level

$$p^*[t; \Lambda^-] - \ln 2\Lambda^- \phi^*[t; \Lambda^-] \leq p^*[t; \Lambda^+] - \ln 2\Lambda^- \phi^*[t; \Lambda^+].$$

Similarly, the optimality of the policy at Λ^+ implies

$$p^*[t; \Lambda^+] - \ln 2\Lambda^+ \phi^*[t; \Lambda^+] \leq p^*[t; \Lambda^-] - \ln 2\Lambda^+ \phi^*[t; \Lambda^-].$$

Summing these two inequalities, we have

$$(\Lambda^+ - \Lambda^-) (\phi^*[t; \Lambda^-] - \phi^*[t; \Lambda^+]) \leq 0.$$

Since $\Lambda^+ > \Lambda^-$, we have $\phi^*[t; \Lambda^-] \leq \phi^*[t; \Lambda^+]$, then $p^*[t; \Lambda^-] \leq p^*[t; \Lambda^+]$ according to (67). Therefore, $\phi^*[t; \Lambda]$ and $p^*[t; \Lambda]$ are strictly increasing over $\Lambda > \iota_n[k, t]$.

To reach the per-slot sum rate in $[\phi^*[t; \Lambda^-], \phi^*[t; \Lambda^+]]$ and power in $[p^*[t; \Lambda^-], p^*[t; \Lambda^+]]$ if $\phi^*[t; \Lambda^-] \neq \phi^*[t; \Lambda^+]$ and $p^*[t; \Lambda^-] \neq p^*[t; \Lambda^+]$, we define the convex combination of $\mathbf{A}^*[t; \Lambda^-]$ and $\mathbf{A}^*[t; \Lambda^+]$ as

$$\mathbf{A}^\xi[t; \Lambda] = \xi \mathbf{A}^*[t; \Lambda^-] + (1 - \xi) \mathbf{A}^*[t; \Lambda^+],$$

and prove that $\mathbf{A}^\xi[t; \Lambda]$ is optimal for any ξ .

Since $p^*[t]$ and $\phi^*[t]$ are linear combinations of continuous terms $\{\bar{c}_n^*[k, t; \Lambda]\}$ and $\{p_n^*[k, t; \Lambda]\}$, thus

$$P_{\text{ext}}[t; \Lambda, \xi] - \ln 2\Lambda \phi^*[t; \Lambda, \xi] = p^*[t; \Lambda] - \ln 2\Lambda \phi^*[t; \Lambda] \quad (68)$$

where

$$\begin{aligned} P_{\text{ext}}[t; \Lambda, \xi] &\triangleq \xi \sum_{n \in \mathcal{N}, k \in \mathcal{K}} p_n^*[k, t; \Lambda] a_n^*[k, t; \Lambda^-] \\ &\quad (1 - \xi) \sum_{n \in \mathcal{N}, k \in \mathcal{K}} p_n^*[k, t; \Lambda] a_n^*[k, t; \Lambda^+] \\ &\stackrel{(a)}{=} \xi \sum_{n \in \mathcal{N}, k \in \mathcal{K}} p_n^*[k, t; \Lambda^-] a_n^*[k, t; \Lambda^-] \\ &\quad (1 - \xi) \sum_{n \in \mathcal{N}, k \in \mathcal{K}} p_n^*[k, t; \Lambda^+] a_n^*[k, t; \Lambda^+] \\ &= \xi p^*[t; \Lambda^-] + (1 - \xi) p^*[t; \Lambda^+], \end{aligned}$$

with (a) holds because $p_n^*[k, t; \Lambda]$ is continuous over Λ . Similarly,

$$\Phi_{\text{ext}}[t; \Lambda, \xi] = \xi \phi^*[t; \Lambda^-] + (1 - \xi) \phi^*[t; \Lambda^+].$$

Thus, $\mathbf{A}^\xi[t; \Lambda]$ is optimal to problem (62) because it has the same optimal value as (68), $P_{\text{ext}}[t; \Lambda, 0] = p^*[t; \Lambda^-]$ and $P_{\text{ext}}[t; \Lambda, 1] = p^*[t; \Lambda^+]$.